

Bonriki Inundation Vulnerability Assessment

Inundation Modelling of Bonriki Islet, Tarawa, Kiribati



Herve Damlamian, Cyprien Bosserelle, Jens Kruger,
Amrit Raj, Zulfikar Begg, Saleshe Kumar, Ryan Lowe,
Mark Buckley, Aseri Baleilevuka



Australian Government



SPC
Secretariat
of the Pacific
Community



Australian
Aid 

Bonriki Inundation Vulnerability Assessment (BIVA)

Inundation Modelling of Bonriki Islet, Tarawa, Kiribati

Herve Damlamian

Cyprien Bosserelle

Jens Kruger

Amrit Raj

Zulfikar Begg

Salesh Kumar

Ryan Lowe

Mark Buckley

Aseri Baleilevuka



©Copyright Secretariat of the Pacific Community (SPC) 2015

All rights for commercial / for profit reproduction or translation, in any form, reserved. SPC authorises the partial reproduction or translation of this material for scientific, educational or research purposes, provided that SPC and the source document are properly acknowledged. Permission to reproduce the document and/or translate in whole, in any form, whether for commercial / for profit or non-profit purposes, must be requested in writing. Original SPC artwork may not be altered or separately published without permission.

Original text: English

Secretariat of the Pacific Community Cataloguing-in-publication data

SPC Technical Report SPC00007

May 2015

SPC DISCLAIMER

While care has been taken in the collection, analysis, and compilation of the data, they are supplied on the condition that the Secretariat of Pacific Community shall not be liable for any loss or injury whatsoever arising from the use of the data.

Secretariat of the Pacific Community
Geoscience Division (GSD)
Private Mail Bag, GPO Suva, Fiji Islands
Telephone: (679) 338 1377
Fax: (679) 337 0040
Email: jensk@spc.int
www.spc.int
www.gsd.spc.int

This report has been produced with the financial assistance from the Secretariat of the Pacific Community.

Table of Contents

Acknowledgements	iv
List of Abbreviations	v
Executive Summary	vi
1. Introduction	7
1.1. Background	7
1.2. Purpose of this report	8
1.3. Scope of this report.....	9
2. Oceanographic Processes	10
3. XBeach Model	11
4. Oceanographic Data Collection	13
5. Calibration.....	19
5.1. One dimension	19
5.2. Two dimensions	22
6. Validation – March 2014 swell event.....	25
6.1. The event	25
6.2. Inundation data collection	29
6.3. Validation of the XBeach model.....	30
7. Results.....	35
7.1. Impact groups	35
7.2. Impact of sea level rise.....	47
7.3. Shoreline vulnerability and inundation pathways	48
7.4. Storm tide versus wave height, the dominant contributor to inundation.....	52
8. Conclusion.....	1
9. References	2

List of Tables

Table 1. Details of deployed oceanographic instruments.	13
Table 2. Comparison between observed and simulated inundation at location 1.	31
Table 3. Comparison between observed and simulated inundation at location 2.	32
Table 4. Comparison between observed and simulated inundation at location 3.	32
Table 5. Comparison between observed and simulated inundation at location 4.	33
Table 6. Comparison between observed and simulated inundation at location 5.	33
Table 7. Comparison between observed and simulated inundation at location 6.	34
Table 8. 2064 Sea level rise (SLR) projections for Tarawa.	35

List of Figures

Figure 1. Bonriki Water Reserve Location.	8
Figure 2. Bonriki Inundation Vulnerability Assessment project components.	9
Figure 3. Location of instruments overlayed with RTK data density.	14

Figure 4. Elevation with respect to mean sea level datum at locations of the reef flat sensors. Sensors g1, g2 and g3 are on the reef slope and not accessible with RTK; an arbitrary elevation was attributed to them for presentation purposes.....	14
Figure 5. Offshore wave and tide conditions during instrument deployment. From top to bottom: root mean square wave height (H_{rms}) in the sea swell (SS: $\frac{1}{2} T_p$ to 1 Hz) and infragravity (IG: 0.00027 Hz to $\frac{1}{2} T_p$) bands, peak period (T_p), peak direction and tidal level at sensor location 1. The x axis shows time in a month/day format for the year 2013.	15
Figure 6. Spectrum of sea surface elevation at AWAC and sensor 6 when wave height is highest.	16
Figure 7. Scatter plot of short-swell root mean square wave height on the reef flat at sensor locations 5, 6 and 8 as a function of offshore short-swell root mean square wave height (at sensor 1) and tidal level (colour).....	17
Figure 8. Scatter plot of infragravity root mean square wave height on the reef flat at sensor locations 5, 6 and 8 as a function of offshore short-swell root mean square wave height (at sensor 1) and tidal level (colour).....	17
Figure 9. Total water level (black) at sensor locations 5 (top), 6 (middle) and 8 (bottom) and contribution from wave set-up (red).....	18
Figure 10. Scatter plot of wave set-up on the reef flat at sensor locations 5, 6 and 8 as a function of wave energy and tidal level (colour).....	19
Figure 11. XBeach parameter combinations for one-dimensional calibration.....	21
Figure 12. Root mean square error (RMS) for short-swell significant wave height at sensor 5. The x axis label is a consecutive number that refers to a given set of parameter combinations as per Figure 11. The y axis is the RMS error in meters.	21
Figure 13. Root mean square error (m) for wave set-up at sensor 5.	22
Figure 14. Root mean square error (m) for infragravity wave at sensor 5.	22
Figure 15. 10-m resolution digital terrain model of Bonriki used to calibrate the inundation model.	23
Figure 16. XBeach parameters combinations for one-dimensional calibration.	24
Figure 17. Root mean square error (m) for short wave height at sensor 5 for the 360 XBeach parameter combinations.....	24
Figure 18. Root mean square error (m) for infragravity wave at sensor 5 for the 360 XBeach parameter combinations.....	25
Figure 19. Root mean square error (m) for wave set-up at sensor 5 for the 360 XBeach parameter combinations.....	25
Figure 20. Data recorded during the March 2014 inundation events; significant wave height = blue line, water level offshore = black line; three vertical dashed lines show the inundation events. The y axis shows water level above tide gauge zero, and the x axis shows time in 2014 with a format of day/month.	26
Figure 21. Astronomical tide extracted from the tide gauge data at Betio, Tarawa (Climate and Ocean Support Program in the Pacific), 1993–2014; the red star shows the perigean spring tide of 1 March, 2014, with a level of 1.18 m above mean sea level. The x axis shows time in years, and the y axis shows normalised water levels in metres.....	27
Figure 22. Tidal decomposition of the Betio tide gauge, 1993–2014; the red star shows the contribution of the residual tide (top), surge (middle) and mean level of the sea (MLOS) component (bottom) to the total water level during the 1 March, 2014 inundation event. The x axis shows time in years, and the y axis shows normalised water levels in metres.	27
Figure 23. Empirical cumulative function of the MLOS.	28
Figure 24. Joint probability of wave and storm tide offshore Bonriki; the markers show the three inundation events that occurred at Bonriki in March 2014.	29
Figure 25. Locations where inundation data were collected after the March 2014 swell event.	29
Figure 26. Comparison between the inundation data collected from the 3 March 2014 swell event and the maximum inundation depth generated from the model. See Table 2 for more details at each location.....	30
Figure 27. Community undertaking post-inundation survey; a 50 cm inundation depth was recorded at this house near location 1.	31

Figure 28. Offshore representative inundation map – minor A.	37
Figure 29. Lagoon representative inundation map – minor A.	38
Figure 30. Offshore representative inundation map – minor B.	39
Figure 31. Lagoon representative inundation map – minor B.	40
Figure 32. Offshore representative inundation map – moderate.	41
Figure 33. Lagoon representative inundation map – moderate.	42
Figure 34. Offshore representative inundation map – severe.	43
Figure 35. Lagoon representative inundation map – severe.	44
Figure 36. Offshore representative inundation map – extreme.	45
Figure 37. Lagoon representative inundation map – extreme.	46
Figure 38. Distribution of the offshore scenarios into risk groups.	47
Figure 39. Distribution of the lagoon scenarios into risk groups.	47
Figure 40. Distribution of the scenarios into impact groups, depending on their attributed SLR projection.	48
Figure 41. Coastline vulnerability to inundation event.	49
Figure 42. Weighted linear regressions, showing erosion since 1984 at transect 9 (Source: BIVA shoreline change analysis report).....	50
Figure 43. Photo showing erosion scar (>50 cm) on the ocean side of Bonriki.	50
Figure 44. Weighted linear regressions showing accretion since 1943 at transect 25 (Source: BIVA shoreline change analysis report).....	51
Figure 45. Weighted linear regressions showing accretion since 1998 at transect 25 (Source: BIVA shoreline change analysis report).....	51
Figure 46. Offshore side – distribution of the scenarios into impact groups depending on their dominant component; either a high storm tide, a high wave height or a mix of both.....	53
Figure 47. Lagoon-side – distribution of the scenarios into impact groups depending on their dominant component; either a high storm tide, a high wave height or a mix of both.....	53

Acknowledgements

The BIVA project is part of the Australian Government's Pacific-Australia Climate Change Science and Adaptation Planning Program (PACCSAP), within the International Climate Change Adaptation Initiative. The project was developed by the Secretariat of the Pacific Community's (SPC) Geoscience Division (GSD) in partnership with the Australian Government and the Government of Kiribati (GoK).

Key GoK stakeholders that contributed to the implementation of the project were:

- Ministry of Public Works and Utilities (MPWU), in particular the Water Engineering Unit with the MPWU
- The Public Utilities Board (PUB), in particular the Water and Sanitation Division and the Customer Relations Division within the PUB
- The Office of the President, in particular the Disaster Management Office
- The Ministry of Environment, Lands and Agricultural Development (MELAD) Lands Division
- The Ministry of Fisheries and Marine Resources Development (MFMRD) Minerals Division
- Members of the Kiribati National Expert Group on climate change and disaster risk management (KNEG)

The Bonriki Village community members also played a key role in the implementation of the project. Community members participated in the school water science and mapping program, assisted with construction of new piezometers and data collection for the groundwater component, and shared their knowledge and experiences with regards to historical inundation events and coastal processes.

Key technical advisors involved with implementation of the project included:

- Flinders University, Adelaide, Australia
- University of Western Australia, Perth, Australia
- The University of Auckland, Auckland, New Zealand
- United Nations Educational, Scientific and Cultural Organization, Institute for Water Education (UNESCO-IHE), Delft, the Netherlands
- Technical advisors Tony Falkland and Ian White

List of Abbreviations

BIVA	Bonriki Inundation Vulnerability Assessment
C_f	bottom friction
f_w	friction coefficient in the wave action
GPS	Global Positioning System
H_{rms}	Root mean square wave height
H_s	significant wave height
IPCCAR5	Intergovernmental Panel on Climate Change Assessment Report 5
MLOS	mean level of the sea
nuhfac	viscosity coefficient for roller-induced turbulent horizontal viscosity
RCP	Representative Concentration Pathways
RI	return interval
RMS	root mean square
RTK	real-time kinematic
SLR	sea level rise
SPC	Secretariat of the Pacific Community

Executive Summary

As part of the Australian-funded Bonriki Inundation Vulnerability Assessment project, a probabilistic inundation hazard assessment of Bonriki was undertaken. The outcomes of this study will be used in the groundwater component of the project to investigate the vulnerability of the Bonriki water resource.

Coastal inundation is of concern to low-lying islands such as Tarawa, Kiribati. Often coastal inundation is the result of the simultaneous occurrence of several events that raise the water level, including the tide, storm surges, wind set up and wave set up, and infragravity waves.

This report describes the last segment of the Bonriki probabilistic inundation hazard assessment study. It combines outcomes from the reports on topography, bathymetry, oceanography, scenario development and coastline change analysis.

Inundation from 72 probable scenarios was numerically assessed using the open source XBeach model. The scenarios were designed to look at return interval events of 20 years, 50 years and 100 years. The results highlight the relatively low vulnerability of the Bonriki freshwater lens to saltwater intrusion under the current sea level. However, the scenarios also show the high vulnerability of the coastal community to inundation events. Under today's sea level, a 20-year return interval event can trigger inundation more than 20–30 metres inland from the shoreline. A 100-year return interval event under the current sea level would generate inundation similar to the inundation that occurred on 3 March, 2014.

In this study, the impact of three sea level rise projection for 2064 (50 years from the time of writing) were investigated, namely RCP6 and RCP8.5 from the Fifth Assessment Report of the Intergovernmental Panel on Climate Change and the intermediate–high scenario from Parris et al. (2012). This study clearly shows the exacerbation of the inundation risk inherent from sea level rise projection, and that this can pose a significant threat to the water resource of Bonriki. Under the RCP6 climate change scenario, a 20-year return interval event leads to potential flooding impacts on the coastal fringes of the islet of Bonriki. Under the RCP8.5 climate change scenario, a 20-year return interval event leads to a potential impact on the peripheral parts of the freshwater lens. Under the intermediate–high scenario, a 20-year return interval event may lead to a potential significant impact on the freshwater lens.

Finally, this study looks at inundation pathways around Bonriki, highlighting the most vulnerable and more resilient parts of the coastline. However, evidence on the recent erosion and accretion rates gathered from the coastal change analysis demonstrates that inundation risk is likely to change if no measure is taken to stabilise the coastline. The recommendation is that the health of the Bonriki freshwater lens and associated resilience of the coastline is best addressed through the implementation of an integrated coastal zone management (ICZM) plan.

1. Introduction

1.1. Background

The Bonriki Inundation Vulnerability Assessment (BIVA) project is part of the Australian government's Pacific–Australia Climate Change Science and Adaptation Planning Program (PACCSAP), within the International Climate Change Adaptation Initiative. The objectives of PACCSAP are to:

- improve scientific understanding of climate change in the Pacific;
- increase awareness of climate science, impacts and adaptation options; and
- improve adaptation planning to build resilience to climate change impacts.

The BIVA project was developed by the Geoscience Division (GSD) of the Secretariat of the Pacific Community (SPC) in partnership with the Australian government and the Government of Kiribati (GoK).

1.1.1. *Project objective and outcomes*

The BIVA project aims to improve our understanding of the vulnerability of the Bonriki freshwater reserve to coastal hazards and climate variability and change. Improving our knowledge of risks to this freshwater resource will enable better adaptation planning by the GoK.

More specifically, the project has sought to use this knowledge to support adaptation planning through the following outcomes:

- Improved understanding and ability to model the role of reef systems in the dissipation of ocean surface waves and the generation of longer-period motions that contribute to coastal hazards.
- Improved understanding of freshwater lens systems in atoll environments with respect to seawater overtopping and infiltration, as well as current and future abstraction demands, recharge scenarios and land-use activities.
- Enhanced data to inform a risk-based approach in the design, construction and protection of the Bonriki water reserve.
- Increased knowledge provided to the GoK and the community of the risks associated with the impact of coastal hazards on freshwater resources in response to climate change, variability and sea-level rise.

1.1.2. *Context*

The Republic of Kiribati is located in the Central Pacific and comprises 33 atolls in three principal island groups. The islands are scattered within an area of about 5 million square kilometres. The BIVA project focuses on the Kiribati National Water Reserve of Bonriki. Bonriki is located on Tarawa atoll within the Gilbert group of islands in Western Kiribati (Figure 1). South Tarawa is the main urban area in Kiribati, with the 2010 census recording 50,182 people of the more than 103,058 total population (KNSO and SPC 2012). Impacts to the Bonriki water resource from climate change, inundation, abstraction and other anthropogenic influences have potential for severe impacts on

people's livelihood of South Tarawa. The Bonriki water reserve is used as the primary raw water supply for the Public Utilities Board (PUB) reticulated water system. PUB water is the source of potable water use by at least 67% of the more than 50,182 people of South Tarawa (KNSO and SPC 2012). Key infrastructure including the PUB Water Treatment Plant and Bonriki International Airport and residential houses are also located on Bonriki, above the freshwater lens, making it an important economic, social and cultural area for the Republic of Kiribati.

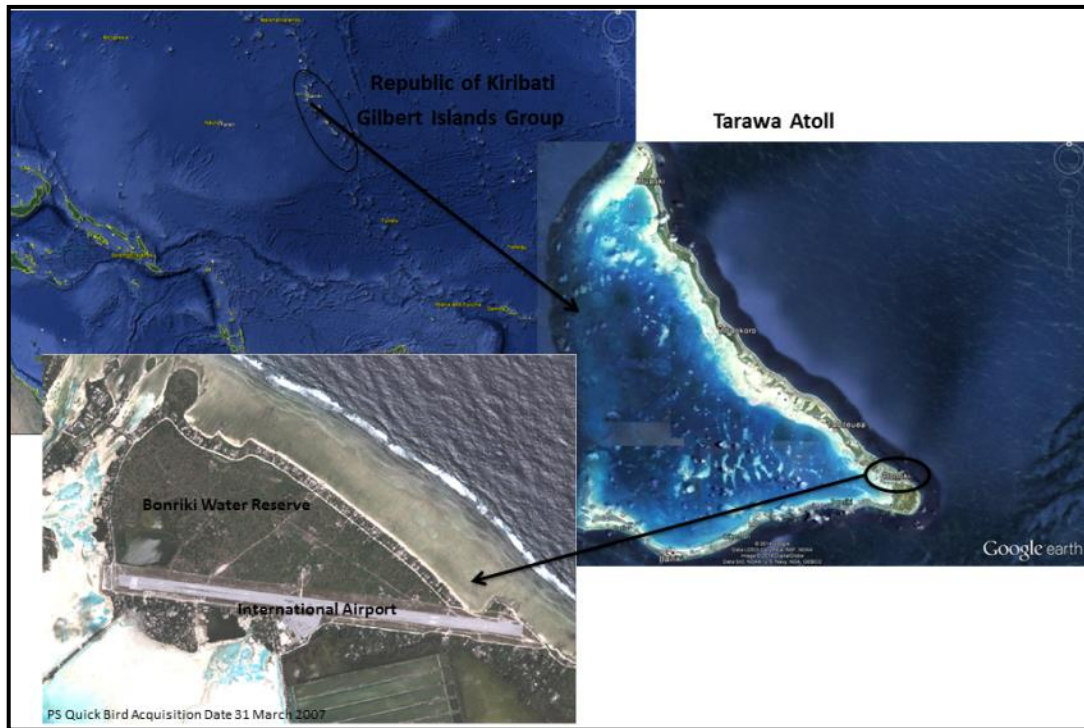


Figure 1. *Bonriki Water Reserve Location.*

1.2. Purpose of this report

This report provides an insight into the development of the inundation model as well as analysing the outcome of the probabilistic inundation hazard assessment of Bonriki. As illustrated in Figure 2, the project has three interlinked components: stakeholder engagement, groundwater investigations and analysis, and coastal investigations and analysis. This report describes the last segment of the Bonriki probabilistic inundation hazard assessment study. It combines outcomes from the topography report, bathymetry report, oceanographic report, the generation of scenarios report and the coastline change analysis report. In turn, the outcome of the coastal work has been used as a baseline for the groundwater modelling activity.

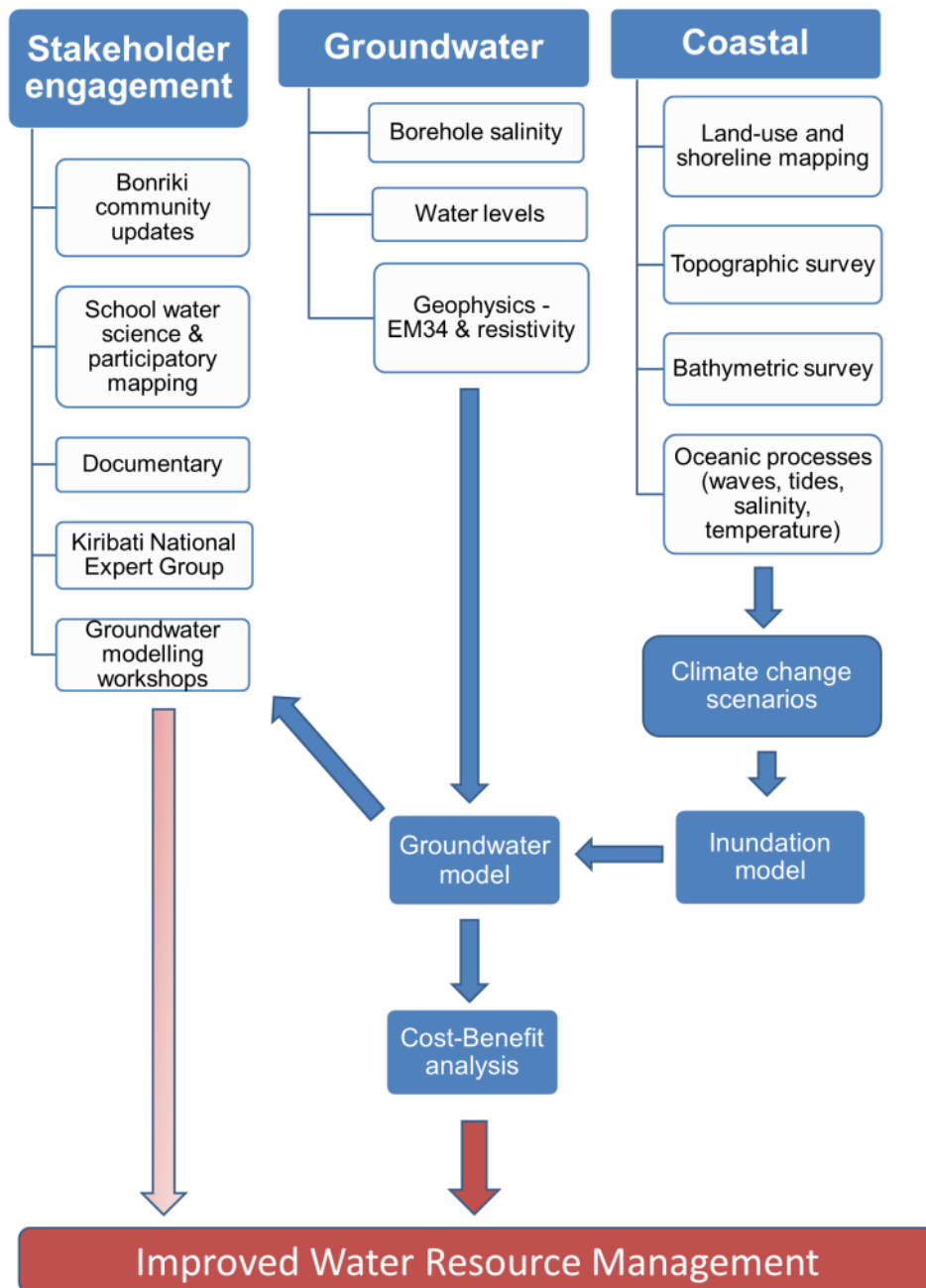


Figure 2. Bonriki Inundation Vulnerability Assessment project components.

1.3. Scope of this report

The coastal activities undertaken as part of the BIVA project, including data collection on topography, bathymetry and oceanography, and the development of possible oceanographic scenarios, were used to develop the inundation model and assess the inundation hazard at Bonriki. This model and assessment are described in detail in this report.

A 10-m grid XBeach model of Bonriki is created and calibrated against the oceanographic data collected on Bonriki (Oceanographic data acquisition report). Once a satisfactory confidence in the model is reached, wave and storm tide condition extracted from the 72 probabilistic scenarios (BIVA Scenario Generation Report) are applied either on the lagoon side or on the ocean side. Finally, a map showing inundation extent and maximum flood depth are derived for each scenario.

This report has the following chapters:

- The chapter on Oceanographic processes describes the dominant oceanographic processes responsible for triggering inundation in an atoll environment. These are provided as background information.
- The chapter on the XBeach model describes some key features of the open source XBeach model, which was used to develop the inundation model.
- The chapter on Oceanographic data collection outlines the activities undertaken during a one-month field investigation, which was done in collaboration with the University of Western Australia.
- The chapter on Calibration provides in-depth details on how the model was calibrated and validated, and discusses the strengths and limitations of the inundation model.
- The Validation chapter describes the March 2014 extreme event and compares model results to ground truth data.
- The chapter on Results presents and discusses the outcomes of the inundation model and attempts to quantify the vulnerability of Bonriki to inundation events.

2. Oceanographic Processes

Inundation as a result of wind-driven storm surge occurs in a continental shelf environment rather than on atolls and, more generally, steep volcanic mid-ocean islands. The contribution of surface wind stress to storm surge is determined by the width and depth of the continental shelf. Atolls have reef-dominated shorelines and lack geomorphic features such as shelves; therefore, the contribution of wind set-up¹ to total surge and subsequent land inundation is minimal. The primary forces driving inundation on reef-fringed coastlines are wave generated, resulting from wave set-up and run-up² as open ocean waves propagate over the reef and onto the land (Dean and Darymple 1991).

The morphology of a typical barrier reef consists of three main sections: a very steep reef slope, a shallow reef flat (<1 m in depth, with a width ranging from tens of metres to hundreds of metres) and a low-lying land area (<5 m in height). As waves propagate over the reef, they undergo several transformations (Lowe and al. 2009). An offshore wave begins shoaling as soon as its wave length is equal to the water depth. This results in energy dissipating from bottom friction and an increase in significant wave height. When the wave height reaches a threshold determined by the ratio of its height to water depth, the wave becomes unstable and breaks. This depth-limited breaking generally occurs when the height of the wave is equal to 78% of the water depth (Dean and Dalrymple 2002). On a fringing reef with a steep outer slope and a shallow reef flat, the surf zone or area where wave breaking occurs is narrow and confined near the reef crest under normal weather conditions. Wave breaking reduces the wave height in the surf zone, which is balanced by a rise in water level, known as wave set-up. This concept is called 'radiation stress', and was developed by Longuet-Higgins and

¹ The increase in the stillwater surface near the shoreline, due to the presence of onshore winds

² The rush of wave water up a slope or structure

Stewart (1962). The remaining waves that propagate onto the reef flat are subject to significant dissipation from bottom friction (Lowe et al. 2009).

The mechanism of swell wave transformation over a fringing reef is a topic of active research. Field studies provide a good understanding of wave transformation into mean wave current over a reef flat due to wave breaking and bottom friction (Lowe et al. 2009; Taebi et al. 2011).

Furthermore, previous studies have shown that the energy spectrum on the reef flat is dominated by motions at the infragravity frequency level (Brander et al. 2004; Lugo-Fernandez et al. 1998; Young 1989;). Those infragravity waves, which are low-frequency waves (0.005–0.04 Hz), are created by the nonlinear interaction of wave groups as bound long waves (Longuet-Higgins and Stewart 1962). More recently, field studies have shown the significant involvement of infragravity waves in the water-level variation on the reef flat (Péquinet et al. 2009). Both studies collected data that suggest that infragravity waves over a reef flat are generated in the surf zone by the radiation stress gradient resulting from the wave group forcing frequencies (Symonds et al. 1982).

Infragravity waves are believed to be major contributor to coastal inundation along reef fringed shorelines. Importantly, infragravity waves are also highly modulated by the water depth on the reef flat. Astronomical tides, storm surge, inter-annual variabilities in the mean level of the sea, and wave set-up can potentially increase water depth over the reef flat, positively influencing the contribution of the infragravity wave. A field study of Ningaloo Reef in Australia showed dominant infragravity waves on the reef flat to be as high as 15% of the incident offshore wave height during high tide (Pomeroy et al. 2012).

3. XBeach Model

A recent and well-tested open source model – XBeach (Roelvink et al. 2010) – was used to develop the inundation model. This included a new process-based and time-dependent two dimensional depth averaged model of the nearshore and coast. XBeach is a good fit for this study because it simulates coupled short-wave energy, flow and infragravity wave generation, propagation and dissipation –processes that take place during an inundation event on an atoll.

A brief description of XBeach is given below, highlighting the key parameters used in this study; an in-depth description can be found in Roelvink et al. (2010).

XBeach solves the time-dependent, short-wave action balance on the scale of wave groups as follows:

$$\frac{\partial A}{\partial t} + \frac{\partial c_x A}{\partial x} + \frac{\partial c_y A}{\partial y} + \frac{\partial c_\theta A}{\partial \theta} = - \frac{D_w}{\sigma}$$

where: A is the action wave, with $A = E_w/\sigma$, where E_w is the wave energy and σ is the intrinsic wave frequency; and c_x and c_y represent the respective components of the wave group velocity.

The velocity in directional space (c_{θ}) takes into account refraction due to the sea bottom and currents. Importantly, energy dissipation due to waves breaking (D_w) is modelled according to Roelvink and Brøker (1993) as:

$$\bar{D}_w = 2 \frac{\alpha}{T_{rep}} Q_b E_w \frac{H_{rms}}{h}$$

with

$$Q_b = 1 - \exp\left(-\left(\frac{H_{rms}}{H_{max}}\right)^n\right), \quad H = \sqrt{\frac{8E_w}{\rho g}}, \quad H_{max} = \frac{\gamma \tanh kh}{k}$$

where: α is the wave dissipation coefficient, E_w is the wave energy, ρ is the density of water, h is the water depth, γ is the breaker index (for calibration), and T_{rep} is the mean period defined by the 1st and 0th moments of the wave spectrum.

Energy dissipation due to bottom friction is:

$$D_f = \frac{2}{3} \rho \pi f_w \left(\frac{\pi H}{T_{rep} \sinh kh} \right)^3$$

where: f_w is the short-wave friction coefficient.

The roller energy balance is coupled to the wave action/energy balance, where dissipation of wave energy is a source for the roller energy balance.

The total roller energy dissipation is given by (Reniers et al. 2004):

$$\bar{D}_r = \frac{2g\beta_r E_r}{c}$$

where: E_r is the roller energy, c is the phase velocity and β is the breaker slope coefficient.

Using these wave action formulations, it is possible to solve directionally spread infragravity waves and time-varying currents.

Surface elevation and flow, including infragravity waves and unsteady wave-induced currents, are solved using the shallow water momentum and mass balance equations. To include short wave-induced mass fluxes and return flows in the shallow water equation, XBeach uses the generalised Lagrangian mean formulation (Andrews and McIntyre 1978).

4. Oceanographic Data Collection

A three-week oceanographic survey took place in November 2013 in collaboration with the University of Western Australia. Twelve oceanographic instruments, including pressure sensors, a directional wave gauge and two Acoustic Doppler Profilers, were deployed to collect wave, water-level and velocity data on the reef slope and the reef flat at Bonriki (Table 1). The location of the instruments is overlaid on a google earth image in Figure 3. Figure 4 shows the height of the instrument as recorded by the real-time kinematic RTK GPS system.

Table 1. Details of deployed oceanographic instruments.

Location name	Latitude	Longitude	Instrument type	Transect	Comment
g01	1.390790	173.151460	Virt D + AWAC	Main	Reef slope ~18 m water depth
g02	1.390200	173.151260	Virt D	Main	Reef slope ~11 m water depth
g03	1.389940	173.150860	Virt D	Main	Reef slope ~5 m water depth
g04	1.388740	173.150040	Virt D	Main	Reef flat nearest reef crest
g05	1.388550	173.149860	Virt D	Main	Reef flat
g06	1.388190	173.149610	Aquadopp HR	Main	Reef flat
g07	1.387540	173.149140	Aquadopp Profiler	Main	Reef flat
g08	1.387040	173.148730	Virt D	Main	Reef flat
g09	1.386630	173.148360	TWR-2050	Main	Reef flat nearest shoreline
g10	1.389221	173.152816	Virt D	South	Reef slope ~11 m water depth
g11	1.387160	173.151060	Virt D	South	Reef flat
	1.389230	173.148090	TWR-2050	North	Instrument failed
	1.418920	172.909660	TWR-2050	Lagoon	Western reef slope
	1.428640	172.969570	Virt D	Lagoon	Lagoon
	1.374200	173.130130	TWR-2050	Lagoon	Bonriki lagoon wharf

Aquadopp HR = Aquadopp high resolution profiler; AWAC = acoustic wave and current meter; TWR = tide and wave recorder; Virt D = virtuoso depth

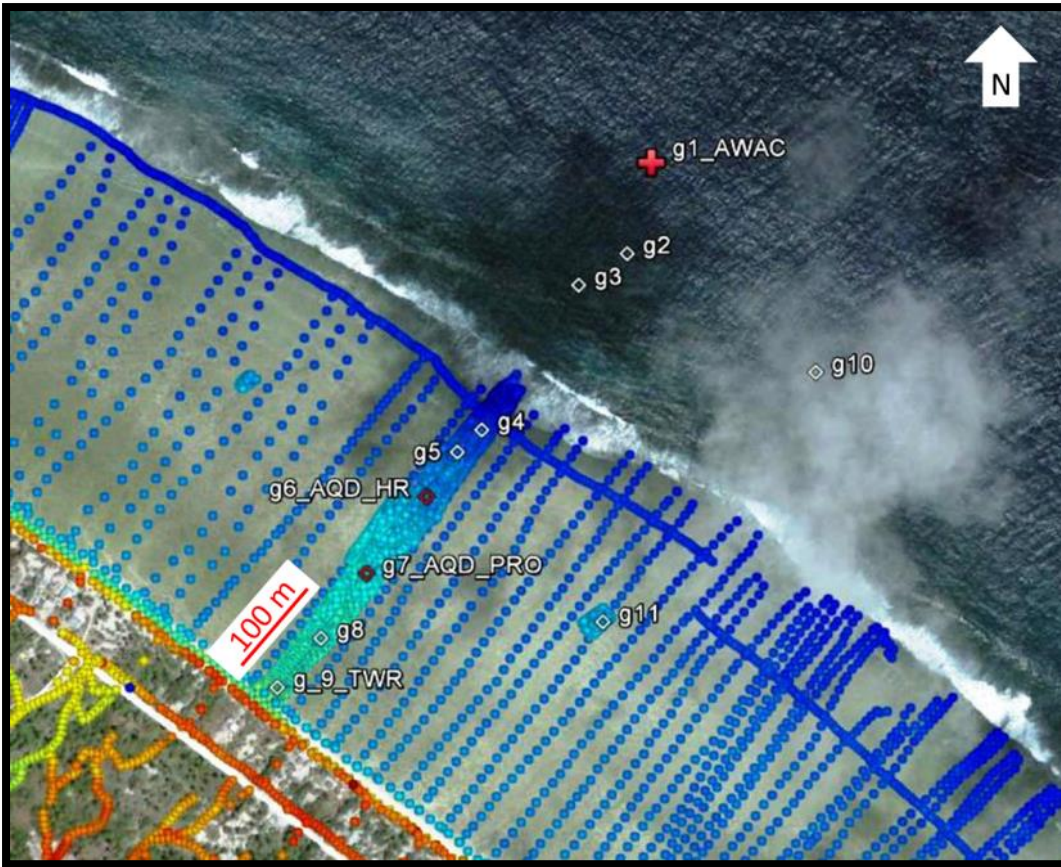


Figure 3. Location of instruments overlaid with RTK data density.

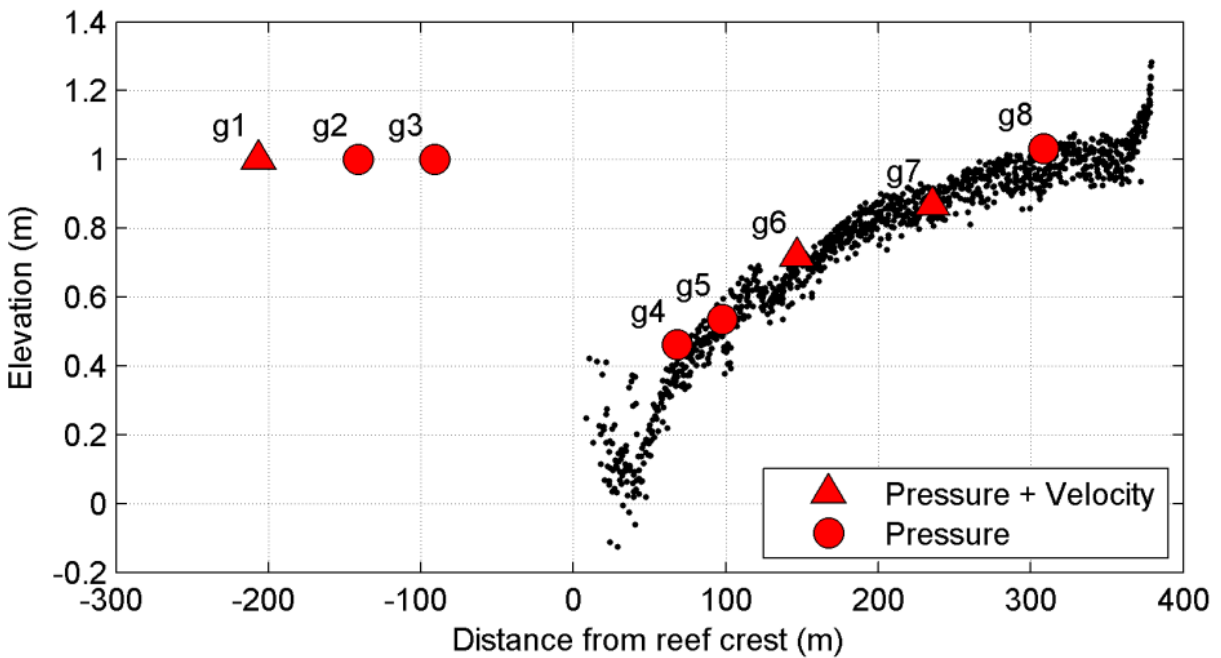


Figure 4. Elevation with respect to mean sea level datum at locations of the reef flat sensors. Sensors g1, g2 and g3 are on the reef slope and not accessible with RTK; an arbitrary elevation was attributed to them for presentation purposes.

The burst data from each pressure sensor were processed to extract short-wave data, wave set-up data and infragravity wave data. These data were used to calibrate the XBeach model. The offshore conditions during deployment of the instruments are shown in Figure 5.

Infragravity waves play a dominant role in triggering inundation events on reef environments. The transformation of the offshore spectral wave to an infragravity wave on the reef flat can be investigated from the various deployed instruments.

A typical wave spectral transformation between offshore and on the reef flat are shown in Figure 6 during the peak of the November 2013 wave event. Short-swell energy dominates the offshore wave spectrum, whereas low frequency, in infragravity or even far infragravity energy, dominates in the reef flat spectrum.

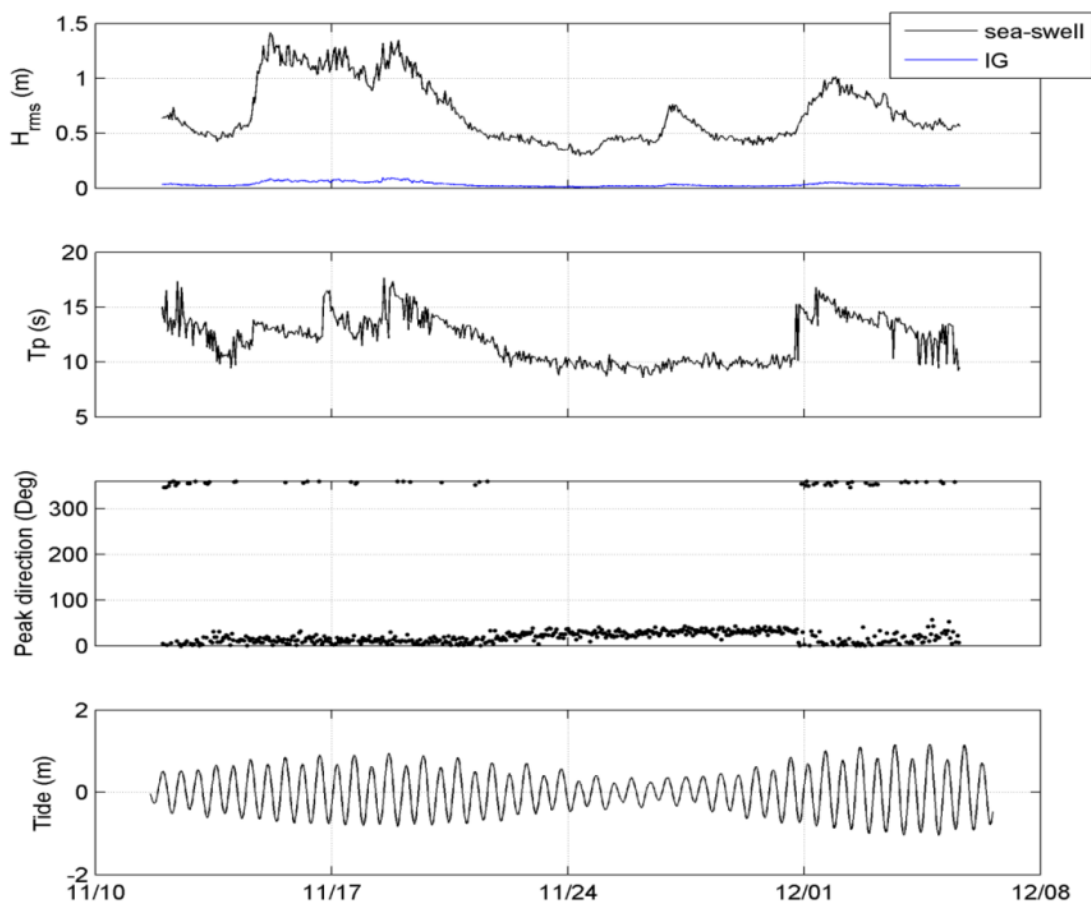


Figure 5. Offshore wave and tide conditions during instrument deployment. From top to bottom: root mean square wave height (H_{rms}) in the sea swell (SS: $\frac{1}{2} T_p$ to 1 Hz) and infragravity (IG: 0.00027 Hz to $\frac{1}{2} T_p$) bands, peak period (T_p), peak direction and tidal level at sensor location 1. The x axis shows time in a month/day format for the year 2013.

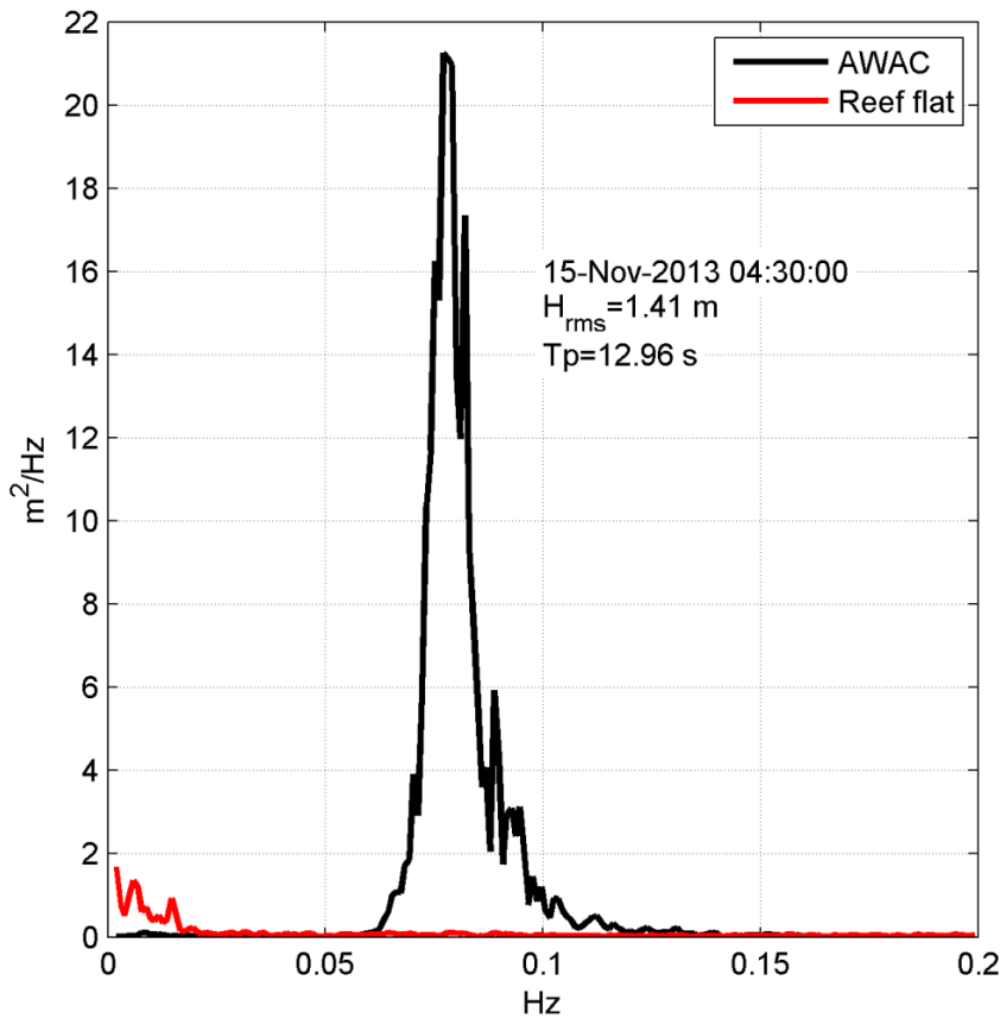


Figure 6. Spectrum of sea surface elevation at AWAC and sensor 6 when wave height is highest.

Wave heights on the reef flat are also tide dependent and consistent with observations on other reefs – that is, larger tidal levels result in larger wave heights. This is true for both short-swell and infragravity bands; although the dependence is more pronounced for the short-swell wave heights (Figure 6 and Figure 7).

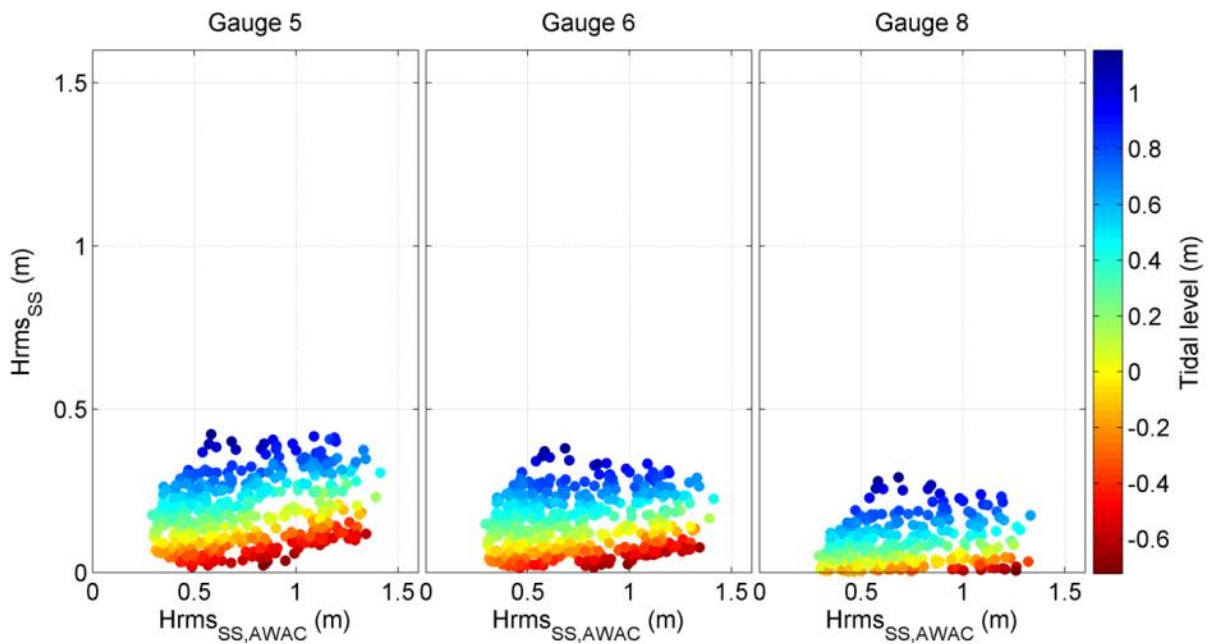


Figure 7. Scatter plot of short-swell root mean square wave height on the reef flat at sensor locations 5, 6 and 8 as a function of offshore short-swell root mean square wave height (at sensor 1) and tidal level (colour).

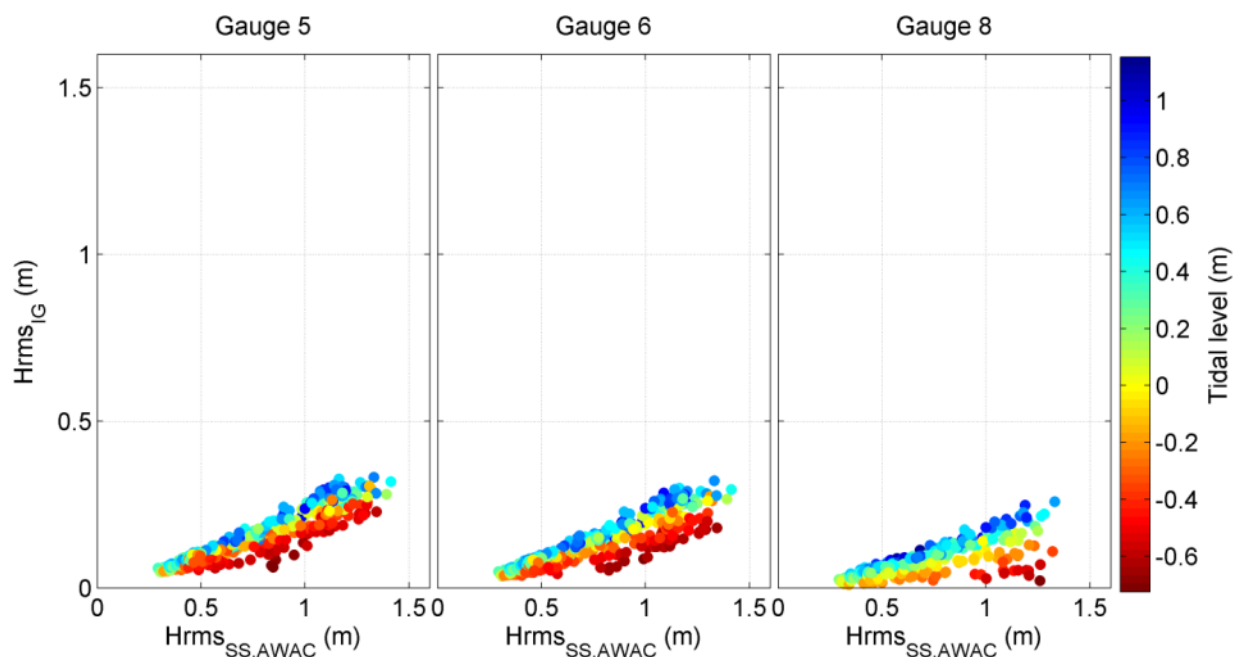


Figure 8. Scatter plot of infragravity root mean square wave height on the reef flat at sensor locations 5, 6 and 8 as a function of offshore short-swell root mean square wave height (at sensor 1) and tidal level (colour).

Wave set-up (h_{setup}) is calculated by estimating a still level (h_{still}), using a linear regression between offshore wave and the water-level difference between offshore and reef flat. The total depth $h_{\text{total}} = h_{\text{still}} + h_{\text{tide}} + h_{\text{setup}}$, where h_{tide} is the tidal level estimated as the demeaned level at sensor 1. Total sea surface elevations on the reef flat at three sensor locations are shown as a time series in Figure 5. Wave set-up shows the expected tidal dependence with larger set-up during low tidal level (Figure 10).

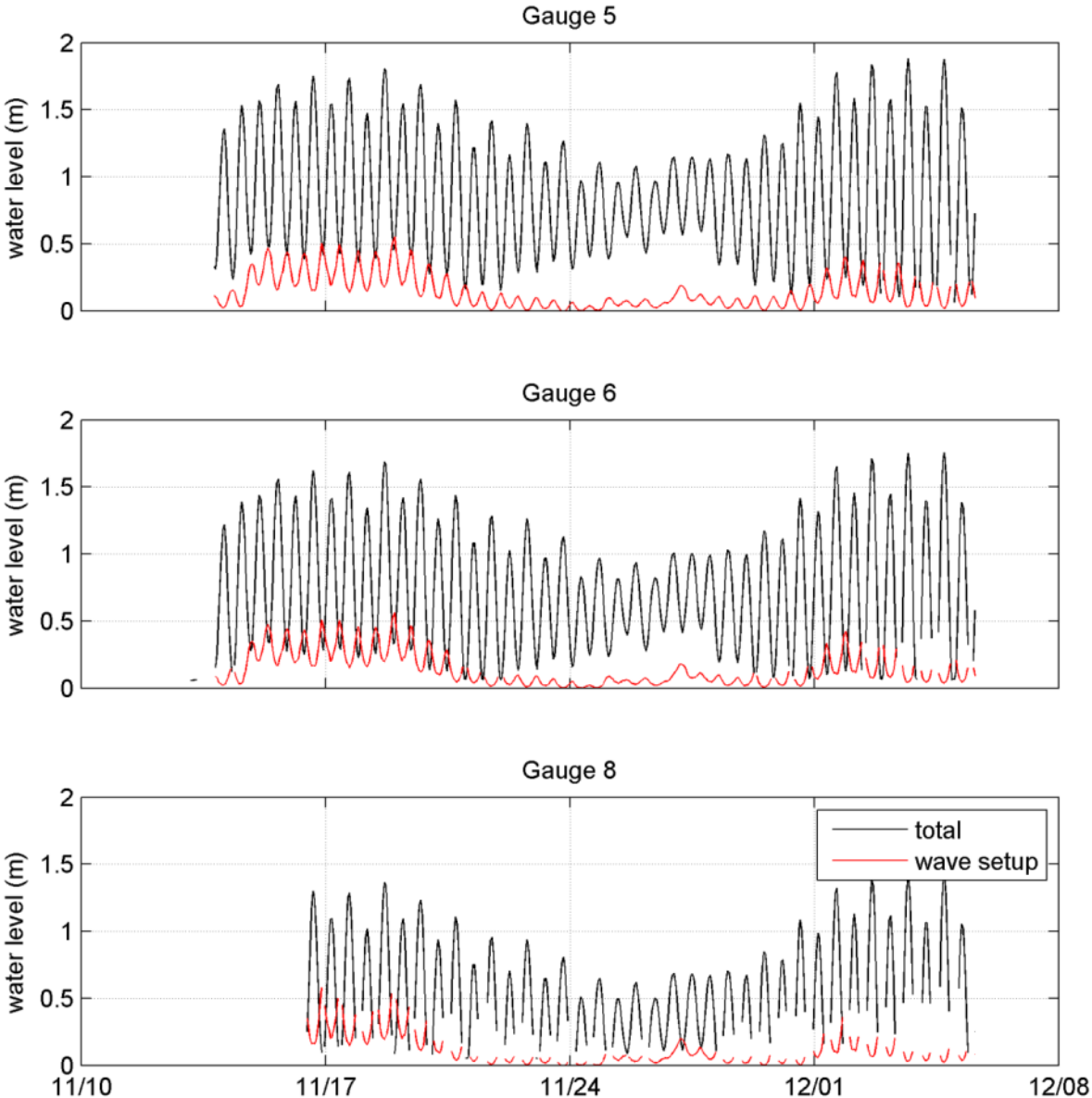


Figure 9. Total water level (black) at sensor locations 5 (top), 6 (middle) and 8 (bottom) and contribution from wave set-up (red).

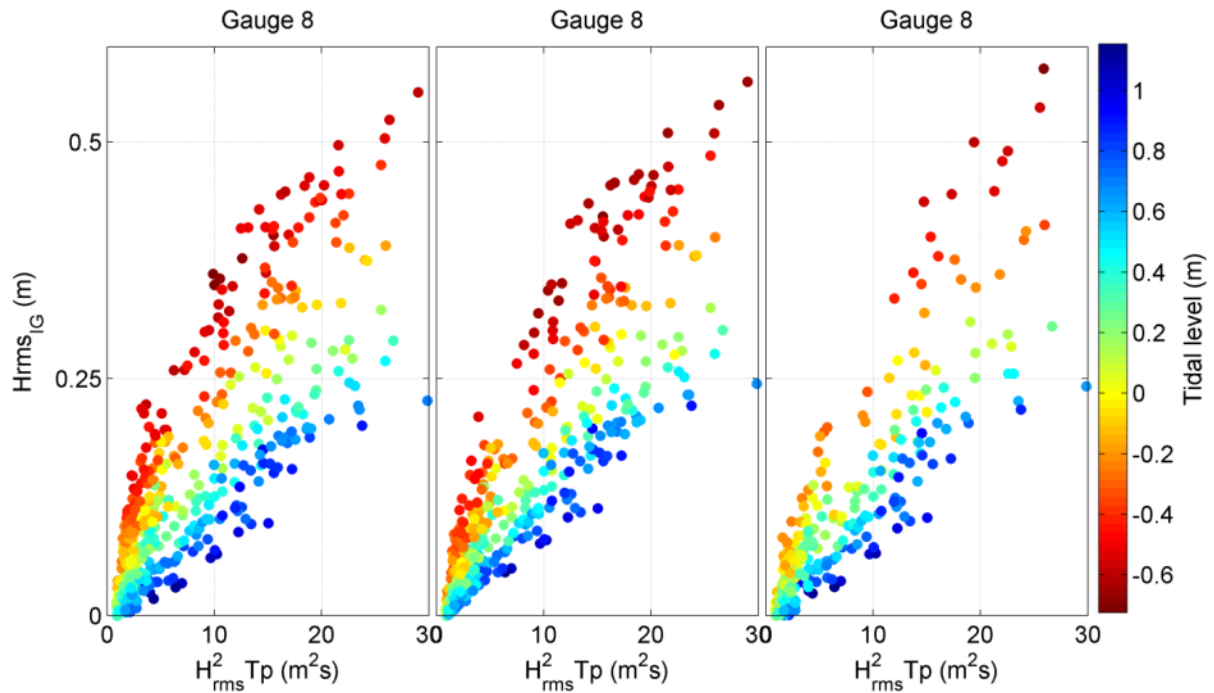


Figure 10. Scatter plot of wave set-up on the reef flat at sensor locations 5, 6 and 8 as a function of wave energy and tidal level (colour).

5. Calibration

The dominant mechanism of wave dissipation across a given fringing reef is dependent on the incident wave height. Lowe et al. (2005) estimated the contribution of incident wave energy dissipated by a barrier reef due to wave breaking and bottom friction separately. They found that the contribution of dissipation by breaking increases with wave height: for small waves (root mean square wave height, or H_{rms} , < 0.6), dissipation by friction accounts for about 80% of total incident wave energy dissipation. For larger waves (significant wave height, or H_s ≥ 1.6), dissipation by breaking becomes dominant, and dissipation by friction only represents about 30% of total incident wave energy dissipation.

This study focuses on relatively large swell events. Wave breaking is, therefore, expected to be the main wave energy dissipation mechanism, even if dissipation by friction is still significant. Thus, data recorded from large-incident wave events were calibrated.

5.1. One dimension

The behaviour of the model is first assessed through a one-dimensional (1D) XBeach model, representing the cross-shore profile in front of Bonriki, where the oceanographic instruments were deployed.

With high confidence in the offshore boundary conditions and the topography profile, respectively, given by the AWAC and a combined RTK GPS and singlebeam survey (BIVA reports on topography

and bathymetry), H_s , wave set-up and the infragravity wave are extracted from the model and compared with the measurements.

Data were calibrated by creating 2,700 combinations of 6 parameters (Figure 11):

- bottom friction (C_f) in the flow equation
- breaker parameter gamma (γ)
- friction coefficient in the wave action (f_w)
- viscosity coefficient for roller-induced turbulent horizontal viscosity (nuhfac)
- breaker slope coefficient (beta)
- fraction of wave height to add onto the water depth in the calculation of energy dissipation (delta).

Each combination of parameters was assessed by modelling the two-largest wave events recorded. The automated calibration process on a 1D profile included 5,400 runs.

The outcome of this 1D calibration was analysed to investigate the behaviour of XBeach. An example of the error analysis for sensor five is given in Figure 12, Figure 13, and Figure 14.

The main findings are detailed below and are similar to results found during a project on the inundation of atolls in French Polynesia (Damlamian et al. 2013).

- The error increases with f_w . This is in agreement with findings from Lowe et al. (2005). An increase in f_w leads to more energy being dissipated by friction, whereas for large waves, dissipation by breaking is dominant.
- For high value of f_w , the influence of gamma is overridden. The influence of wave energy dissipation by breaking decreases relative to dissipation by friction. To be in agreement with Lowe et al. (2005), for large waves, f_w should be constrained below $f_w < 0.5$.
- When the flow and short-wave friction coefficients cf and f_w , respectively, are low, high gamma causes rapid wave energy conversion into set-up, resulting in a divergence in the root mean square error for wave height and wave set-up.

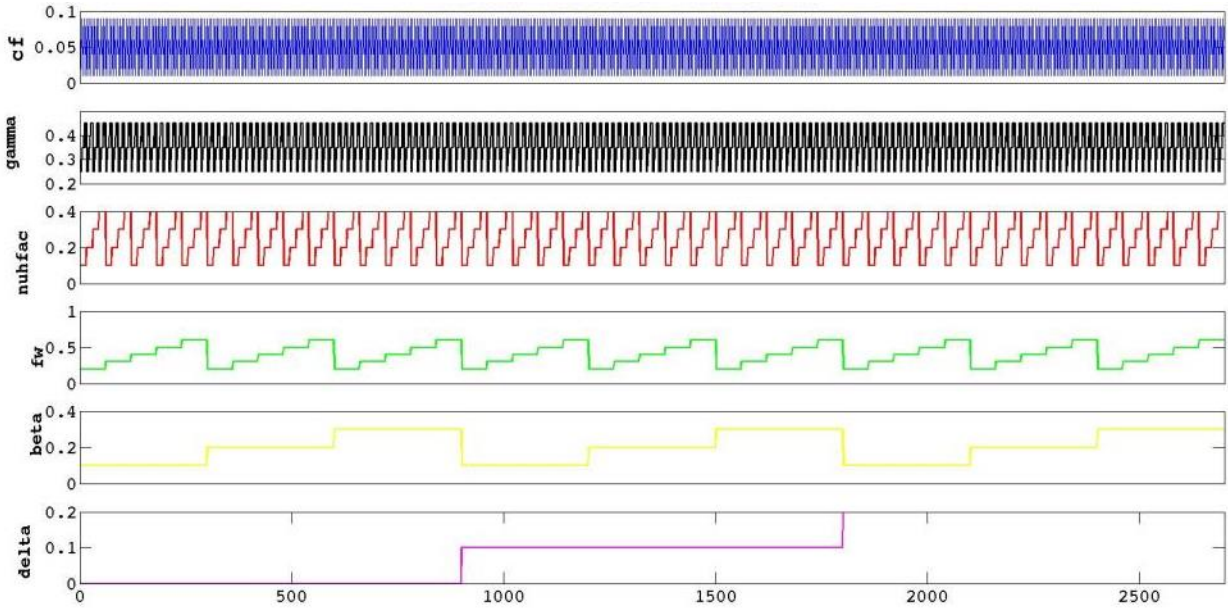


Figure 11. XBeach parameter combinations for one-dimensional calibration.

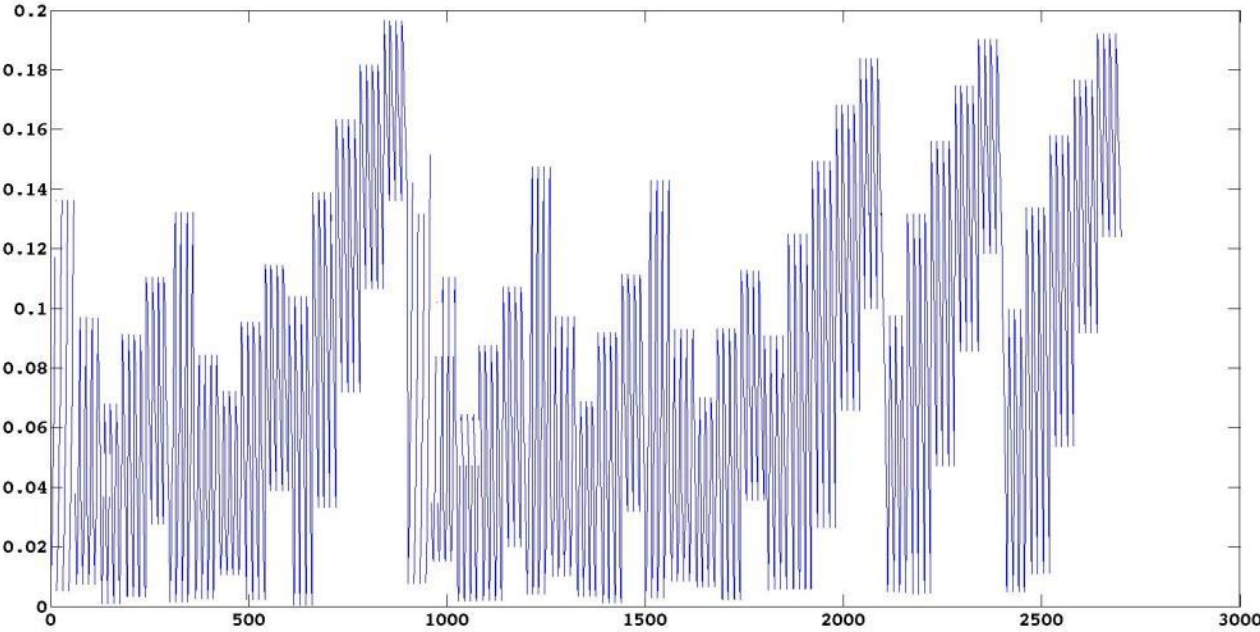


Figure 12. Root mean square error (RMS) for short-swell significant wave height at sensor 5. The x axis label is a consecutive number that refers to a given set of parameter combinations as per Figure 11. The y axis is the RMS error in meters.

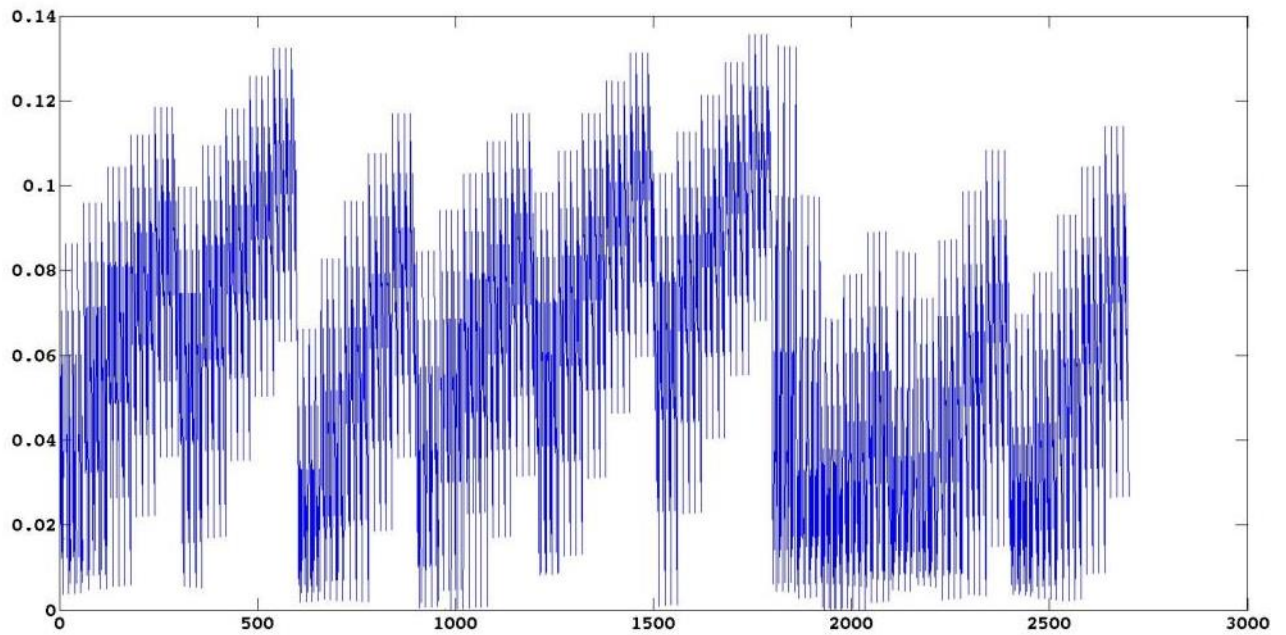


Figure 13. Root mean square error (m) for wave set-up at sensor 5.

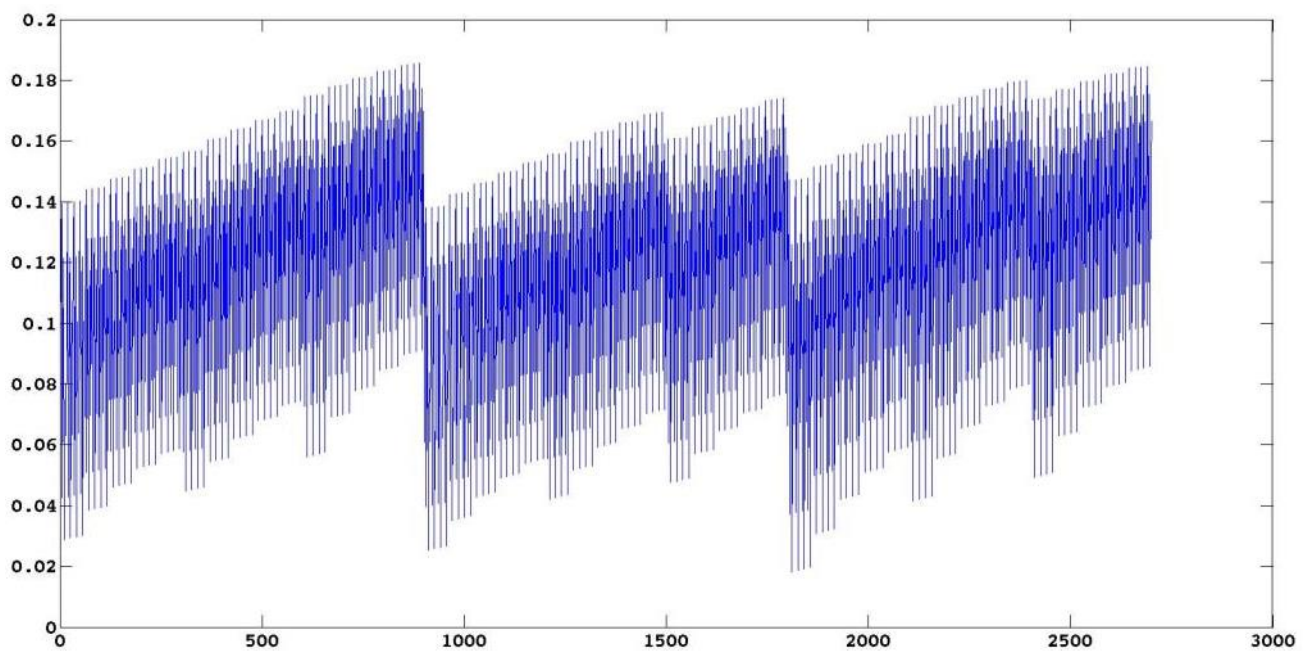


Figure 14. Root mean square error (m) for infragravity wave at sensor 5.

5.2. Two dimensions

A two-dimensional model of Bonriki was developed. Topography and bathymetry data were firstly integrated into a triangular mesh. Each node was then interpolated onto a 10-m rectangular grid. The digital terrain model (Figure 15) was built with various sources of data.

- RTK GPS topography data, as reported in Begg et al. (2015)
- Aerial photo-derived topography data from an unmanned aircraft system survey, as reported in the Begg et al. (2015).

- Singlebeam data, as reported in Kumar (2015).
- Multibeam data collected by SOPAC as part of the EDF8 project (Kruger and Sharma, 2008).

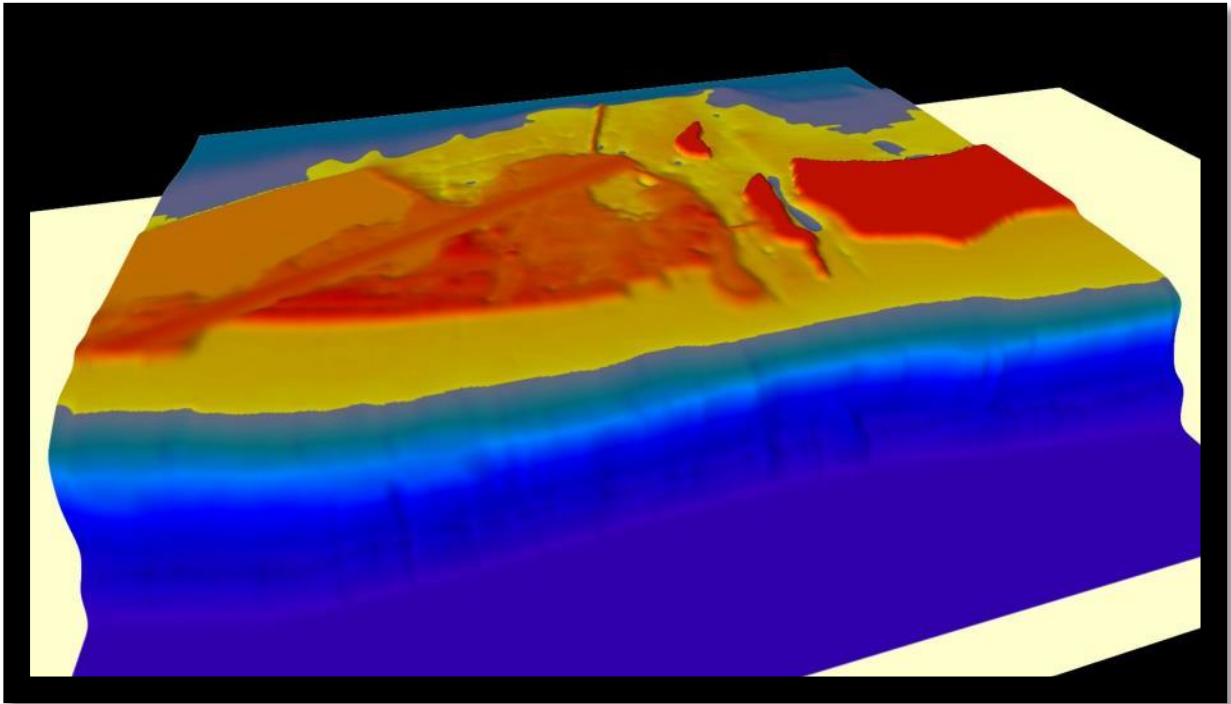


Figure 15. 10-m resolution digital terrain model of Bonriki used to calibrate the inundation model.

The two-dimensional XBeach model requires a relatively high computational time. Guided by the outcome of the one-dimensional calibration, the number of parameter combinations is restricted to 360 (Figure 16).

Calibration involves five parameters: C_f , γ , nuhfac , f_w and δ . The breaker slope coefficient is now fixed to its default value of $\beta = 0.15$.

The 2D model is forced by the directional wave spectrum information and water-level data collected by the AWAC on the reef slope.

Each combination of parameters was assessed by modelling the largest wave event recorded, and by comparing modelled and measured H_s , wave set-up and infragravity wave on the reef flat. An example of the error analysis for sensor five is given in Figure 17, Figure 18, and Figure 19.

Several sets of parameters that were giving reasonable calibration results were extracted. To pick the final set, additional considerations were taken into account.

- Water flow is attenuated on rough bottoms (reef flat and land during inundation) so that C_f needs to be relatively high.
- f_w should be larger than 0 but smaller than 0.5 (Lowe et al. 2005).
- Calibrated parameters should emphasise infragravity wave and wave set-up, rather than wave attenuation.

The chosen combination of parameters is $C_f = 0.01$, $\gamma = 0.55$, $\text{nuhfac} = 0.2$, $f_w = 0.3$ and $\delta = 0.1$. The root mean square error between infragravity waves is relatively high near the reef

crest, with a root mean square of 0.07 m. The root mean square error decreases to 0.022 m at the shore.

The short wave height gives a root mean square error ranging from 0.15 m to 0.06 m across the reef flat. Finally, average root mean square error between observed and simulated wave set-up across the reef flat is 0.021 m.

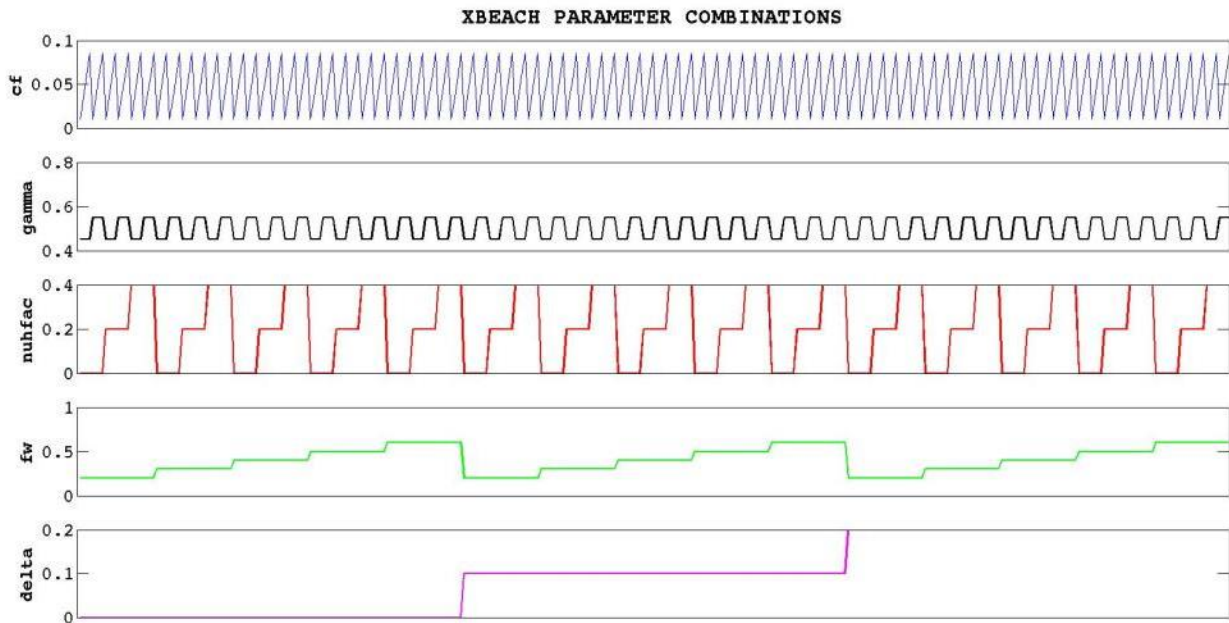


Figure 16. XBeach parameters combinations for one-dimensional calibration.

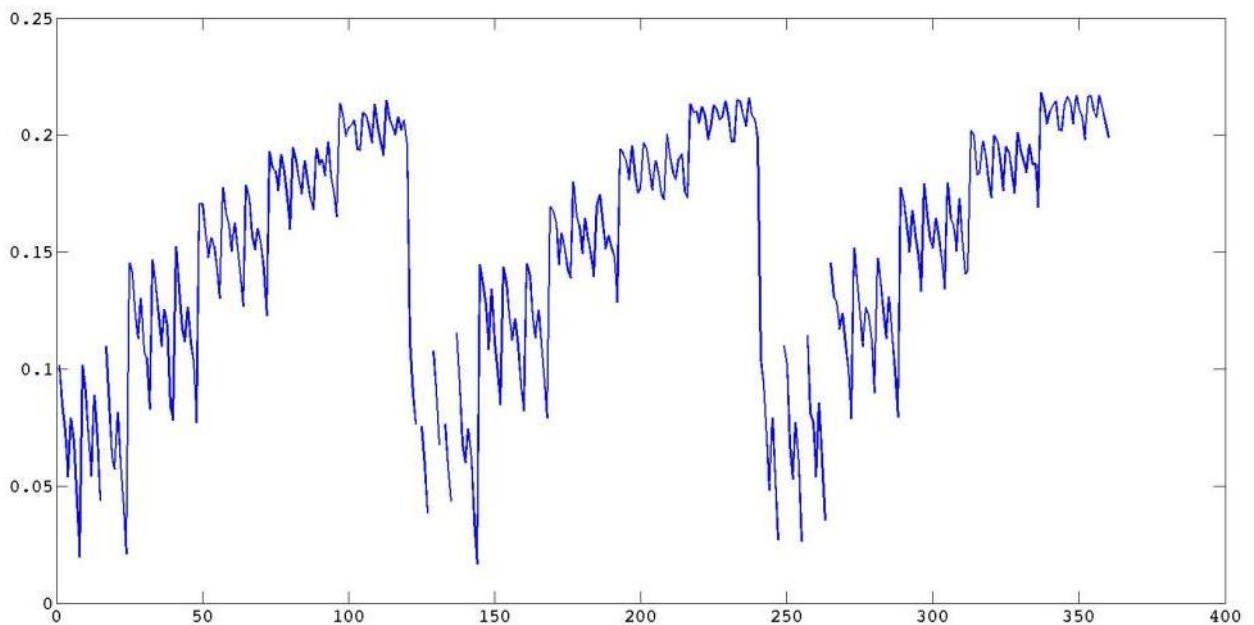


Figure 17. Root mean square error (m) for short wave height at sensor 5 for the 360 XBeach parameter combinations.

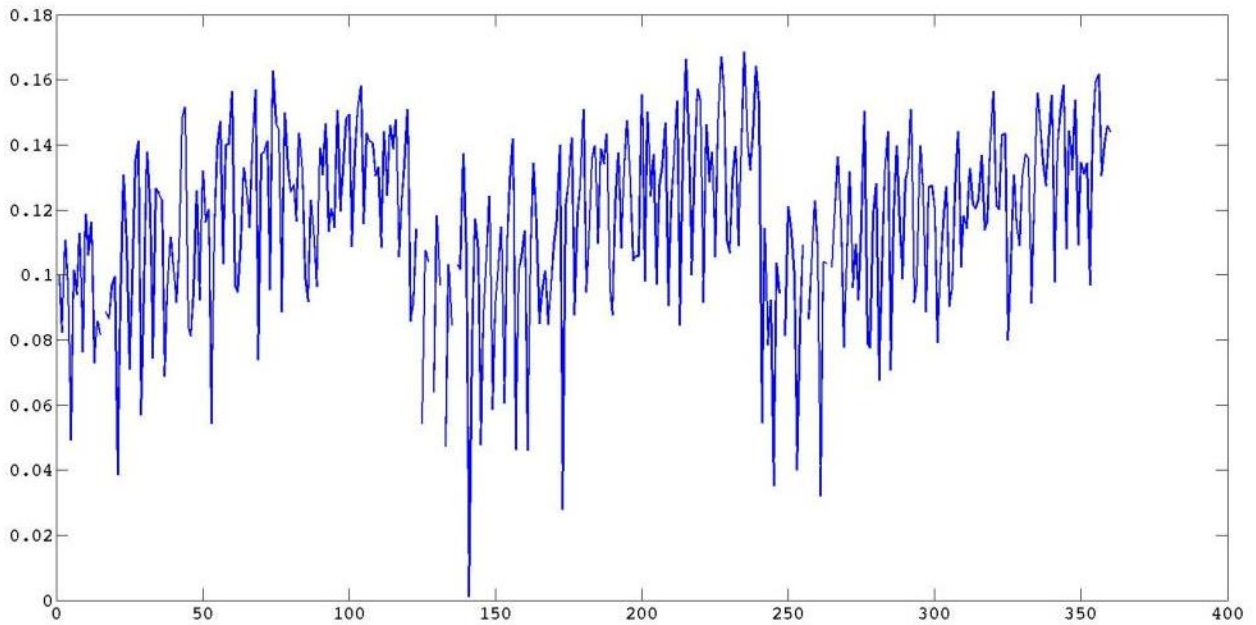


Figure 18. Root mean square error (m) for infragravity wave at sensor 5 for the 360 XBeach parameter combinations.

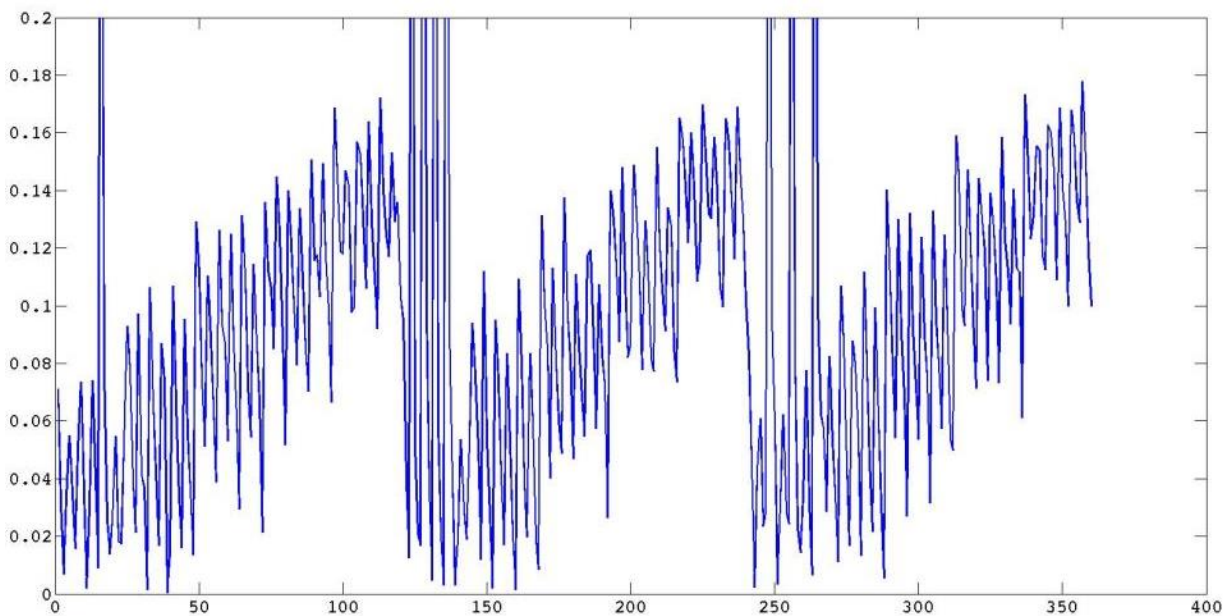


Figure 19. Root mean square error (m) for wave set-up at sensor 5 for the 360 XBeach parameter combinations.

6. Validation – March 2014 swell event

6.1. The event

In early March 2014, an extra tropical storm that developed in the north Pacific generated a large swell that propagated across the ocean in a southward direction. The swell impacted Tarawa on

March 3 and 4. Only one oceanographic instrument was deployed at the time of the impact. The directional wave gauge (AWAC) deployed on the reef slope in front of Bonriki recorded the event, with a maximum significant wave height of 2.5 m. Fortunately, this swell event did not coincide with the perigean spring tide (or king tide), which occurred on 1 March, as a co-occurrence of a perigean spring tide with a large swell event would have led to more severe inundation.

Between 1 March, 2014 and 4 March, 2014, three inundation events were reported in Bonriki. Figure 20 shows the recorded wave height and water level during the events.

On 1 March, inundation occurred from the lagoon side, due to the perigean spring tide. The tide gauge recorded its highest water level since its installation in 1993, with a peak at about 2.7 m above tide gauge zero.

A tidal decomposition, using a wavelet filter, on the tide gauge data provides insight on the different contributors to this extreme water level.

The exceptionally high water level is mainly attributed to the astronomical tide, with a very high spring tide of 1.18 m above mean sea level (Figure 20), combined with a high MLOS of about 0.2 m (Figure 22 and Figure 23).

On the ocean side, no significant inundation was reported on 1 March. The easterly waves were too low ($H_s = 1$ m) to significantly overtop the beach berm.

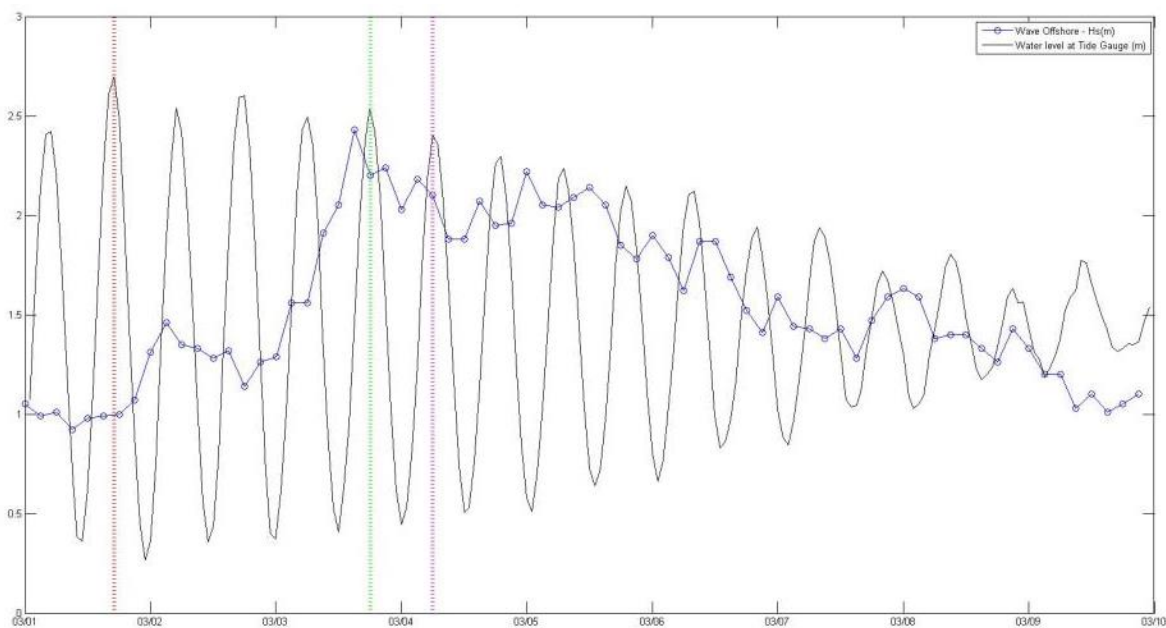


Figure 20. Data recorded during the March 2014 inundation events; significant wave height = blue line, water level offshore = black line; three vertical dashed lines show the inundation events. The y axis shows water level above tide gauge zero, and the x axis shows time in 2014 with a format of day/month.

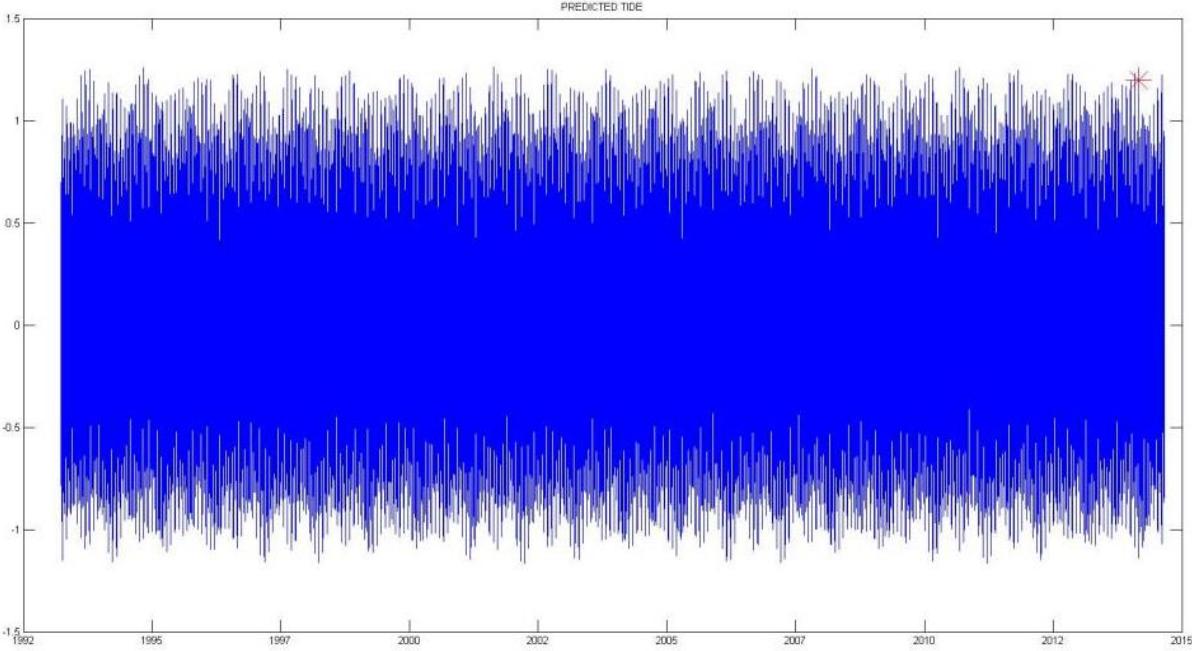


Figure 21. Astronomical tide extracted from the tide gauge data at Betio, Tarawa (Climate and Ocean Support Program in the Pacific), 1993–2014; the red star shows the perigean spring tide of 1 March, 2014, with a level of 1.18 m above mean sea level. The x axis shows time in years, and the y axis shows normalised water levels in metres.

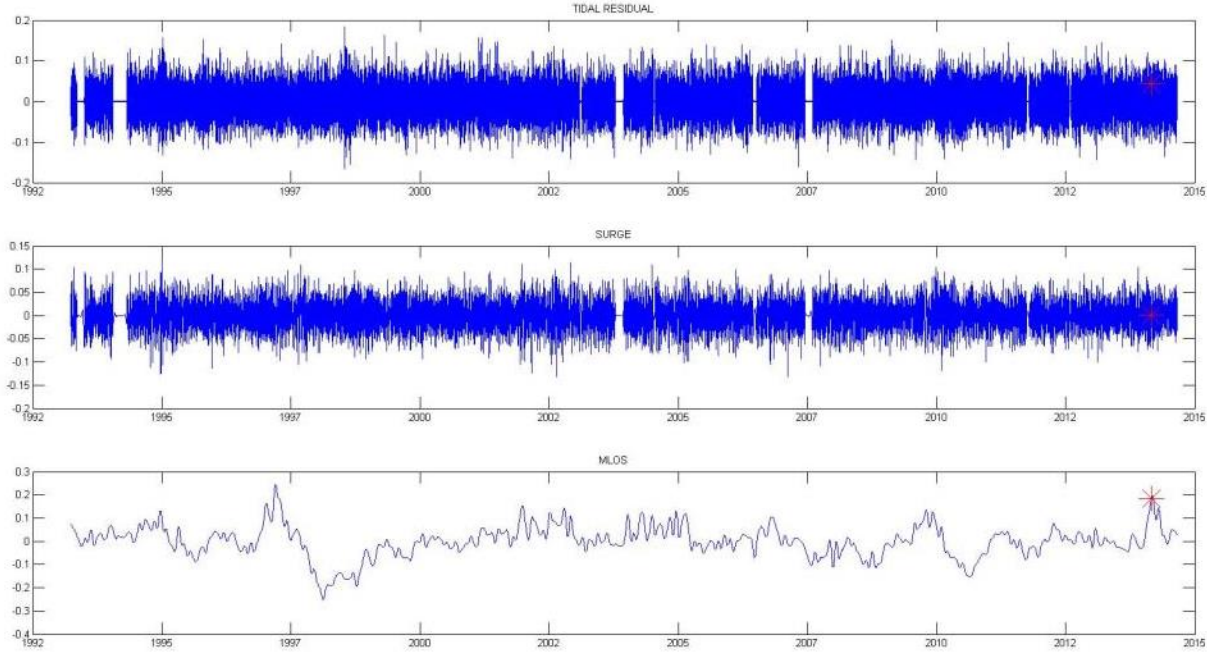


Figure 22. Tidal decomposition of the Betio tide gauge, 1993–2014; the red star shows the contribution of the residual tide (top), surge (middle) and mean level of the sea (MLOS) component (bottom) to the total water level during the 1 March, 2014 inundation event. The x axis shows time in years, and the y axis shows normalised water levels in metres.

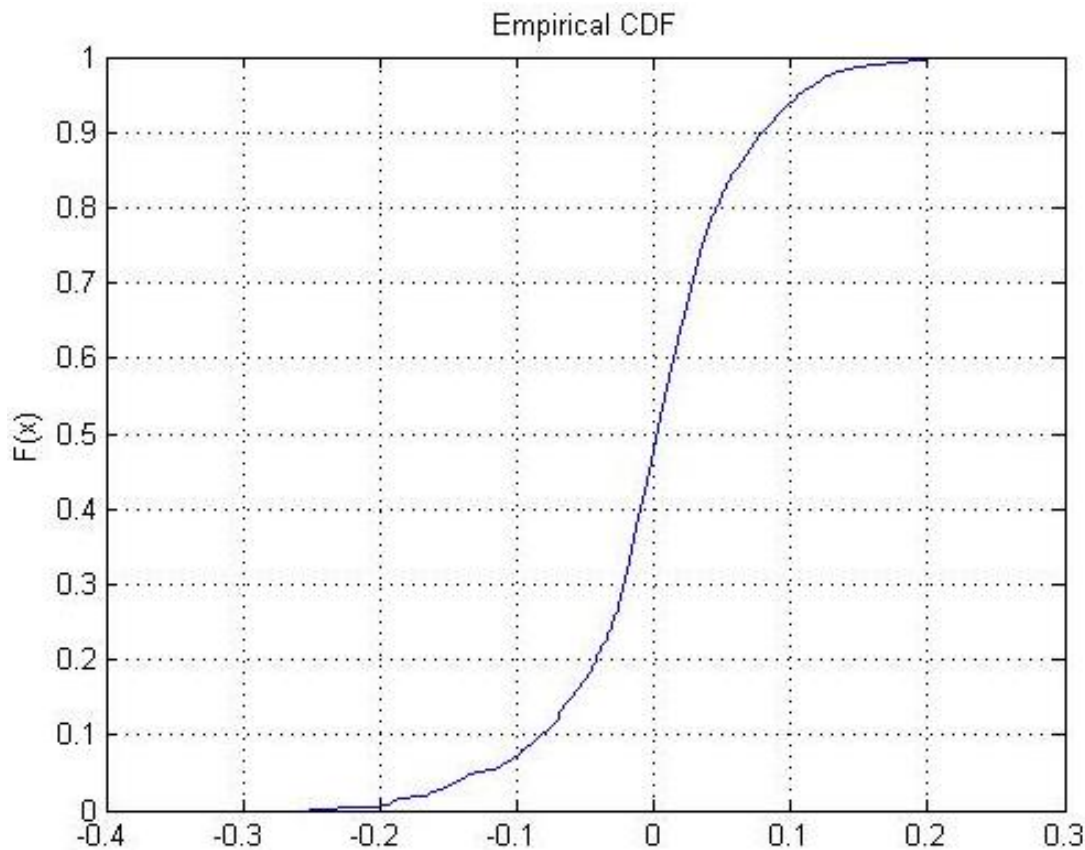


Figure 23. Empirical cumulative function of the MLOS.

Between 3 March, 2014 and 4 March, 2014, the large swell that originated from the northern part of the Pacific Ocean reached Tarawa. The coincidence of this swell event with a high water level created significant inundation on the ocean side. The reported inundation occurred in the evening of 3 March, with a recorded significant wave height of 2.4 m and a recorded water level offshore of 2.5 m. On the next high tide, inundation occurred again, with a wave height of 2.1 m and an offshore water level of 2.4 m.

Based on the outcome of the joint probability of wave and storm tide (BIVA report on severe and extreme scenarios), the three inundations events that occurred between 1 March and 4 March 2014 can be ranked as shown in Figure 24.

- The lagoon water level on 1 March is classified as a 100-year return interval (RI). (On the ocean side, the sea conditions, with a 2.7 m water level and a 1 m wave is ranked as a 200-year RI, but did not generate inundation on the ocean side shoreline)
- On 3 March, the event that combined a 2.5 m water level with a 2.2 m wave height is ranked as a 100-year RI.
- On 4 March, the event that combined a 2.4 m water level with a 2.1 m wave event is ranked as a 20-year RI.

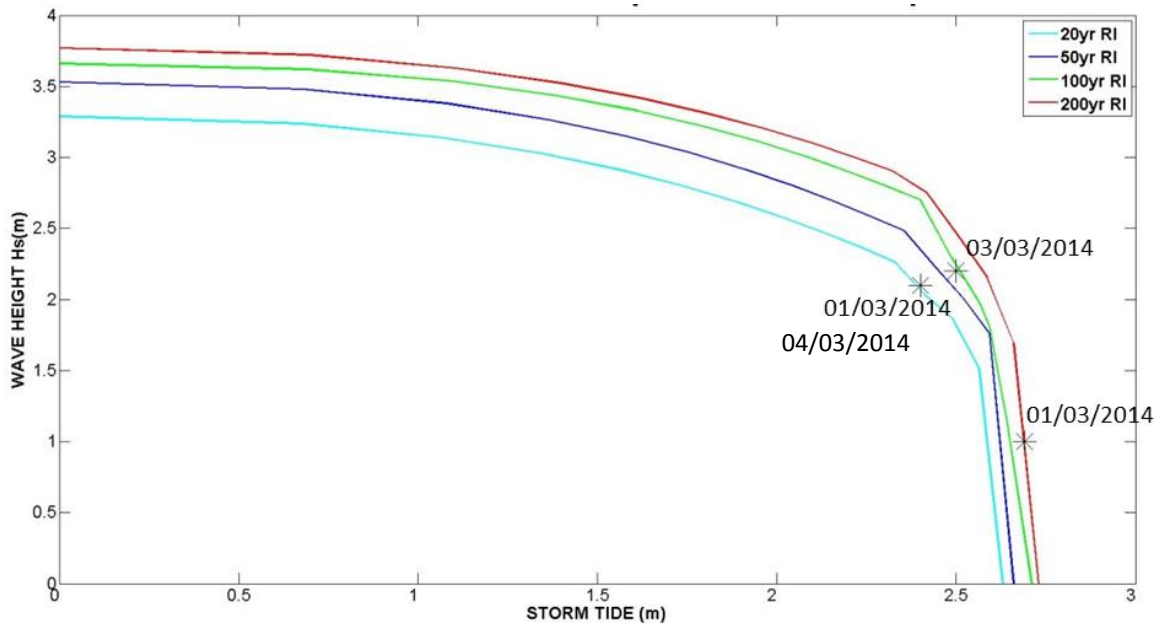


Figure 24. Joint probability of wave and storm tide offshore Bonriki; the markers show the three inundation events that occurred at Bonriki in March 2014.

6.2. Inundation data collection

On 4 March, the BIVA team conducted a post-inundation survey, collecting inundation depth and inundation extent data from six locations around Bonriki (Figure 25). The data were sourced from witness testimony and cross-checked with evidence left by the event (i.e. debris), when possible.

Information sourced from the community was very valuable because it helped our understanding of the different mechanisms involved in the March events. The worst inundation was recorded as originating from the 3 March, and was experienced on both side of the islet – on the ocean side and on the lagoon side.

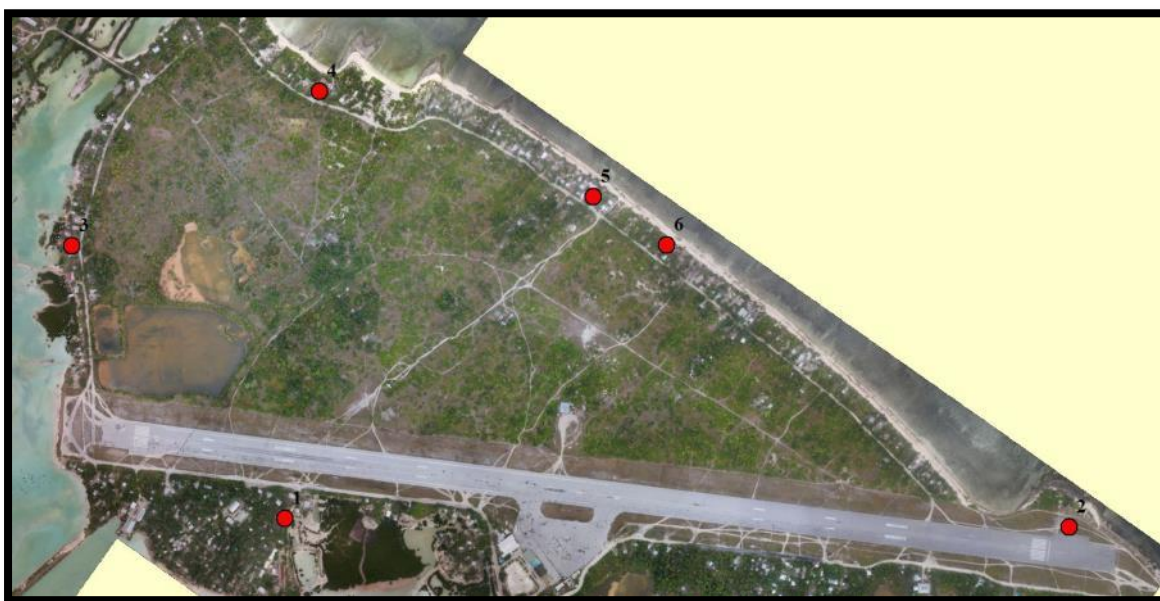


Figure 25. Locations where inundation data were collected after the March 2014 swell event.

6.3. Validation of the XBeach model

The XBeach model was calibrated with measurements collected on the reef flat. The calibrated model of Bonriki was tested against the inundation data collected from the 3 March swell event. As described in the introductory section above, inundation heavily depends on the topography data and the bottom friction (C_f). With a fixed C_f , the model is developed with the conservative assumption that water is flowing on bare land, potentially increasing the inundation extent.

The model was forced with the spectral wave and the water-level information collected on the reef slope by the AWAC. The model output was then processed into a map of maximum inundation depth, allowing straight comparison with the inundation data collected (Figure 26).

Overall, the modelled inundation compares well with the post-inundation data collected from the 3 March event. The model shows wet cells (land submersed under water) in each part of the shoreline where inundation was reported. Noticeable discrepancies can be either largely attributed to the inaccuracy of the topography data or the possible inaccuracy of the testimony collected after the event.

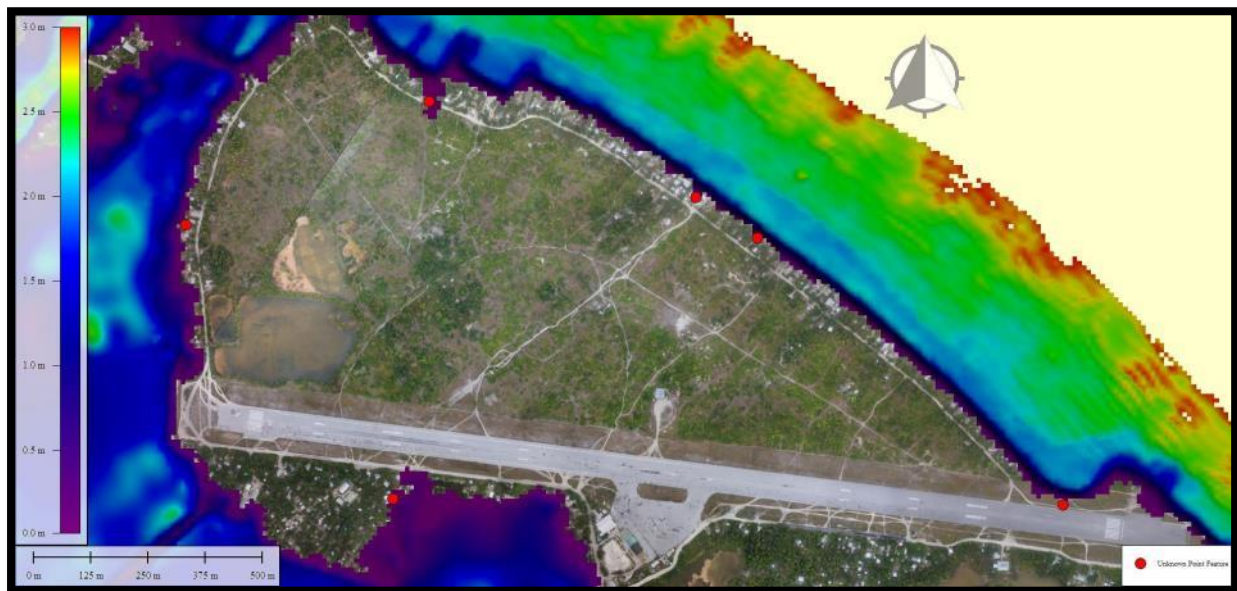


Figure 26. Comparison between the inundation data collected from the 3 March 2014 swell event and the maximum inundation depth generated from the model. See Table 2 for more details at each location.

At location 1, on the lagoon side, two inundation depths were recorded (Table 2). The observation closer to shore is in good agreement with the model, with an inundation depth lower than 10 cm. The second inundation depth observation of 50 cm was recorded on the wall of a house located across the road (Figure 27). The model only shows a 5 cm inundation depth at that same location. Taking into account the location of the house, the surrounding flat topography and the lack of evidence shown at the measurement site (Figure 27), the discrepancy could potentially come from the uncertainty in the data collected from a witness account.

Table 2. Comparison between observed and simulated inundation at location 1.


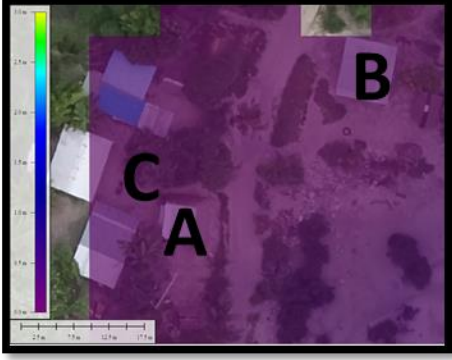

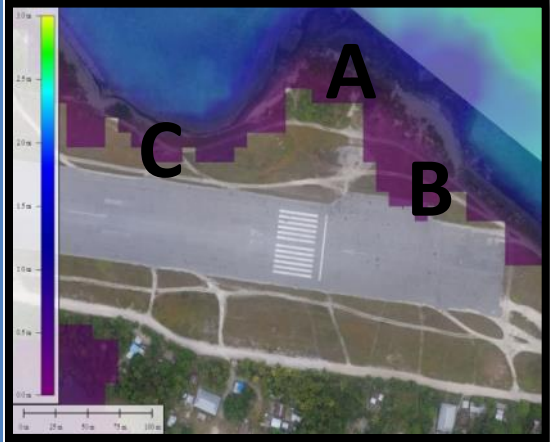
Location 1	Observed	Modelled
Image		
Details	<ul style="list-style-type: none"> • Sea water went across the road to location C • Water reached building B, but not above bricks (<10 cm). • Water reached house A with a water level of about 50 cm (Figure 27) 	<ul style="list-style-type: none"> • Inundation extent crossed the road to location C • Inundation depth in front of house B is 10 cm • Inundation depth in front of house A is 5 cm



Figure 27. Community undertaking post-inundation survey; a 50 cm inundation depth was recorded at this house near location 1.


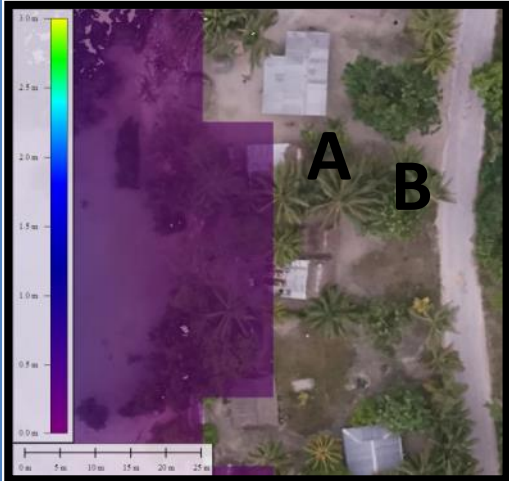
No inundation depth data were collected at location 2 (Table 3).

Table 3. Comparison between observed and simulated inundation at location 2.

Location 2	Observed	Modelled
Image		
Details	<ul style="list-style-type: none"> • Seawall overtopped • Sea water almost reached the runway 	<ul style="list-style-type: none"> • Seawall was overtopped (A and B) • Sea water almost reached the runway (B and C)

In location 3, the topography data from RTK GPS is very sparse, while the topography data derived from the unmanned aircraft vehicle are of poor quality, as discussed in the BIVA topography report. The poor baseline data around location 3 can explain the difference between the simulated (16 cm) and observed (45 cm) inundation depths (Table 4).

Table 4. Comparison between observed and simulated inundation at location 3.

Location 3	Observed	Modelled
Image		
Details	<ul style="list-style-type: none"> • Taanea causeway submerged, residents describe the water coming in as a tsunami like surge. • Breadfruit in A shows evidence of salt water • Sea water almost reached the road • Inundation depth ~45 cm 	<ul style="list-style-type: none"> • Causeway is submerged • Inundation stopped 6 m from the breadfruit (or one-grid cell) • Inundation did not reach the road • Inundation depth 16 cm at the house near the breadfruit (A)

On the ocean side, locations 4, 5 and 6 show good agreement with the collected inundation depth data (Tables 5–7).

Table 5. Comparison between observed and simulated inundation at location 4.


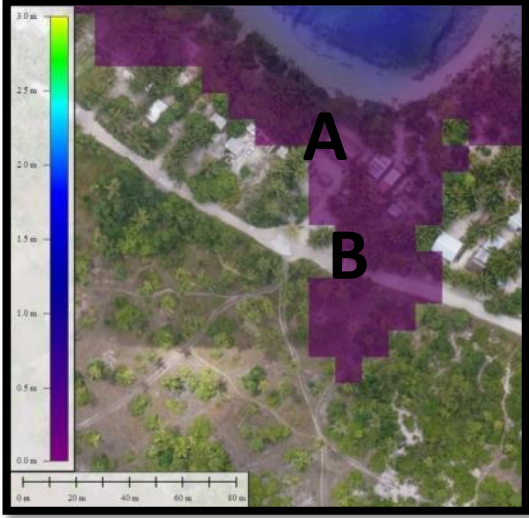
Location 4	Observed	Modelled
Image		
Details	<ul style="list-style-type: none"> • Water reached the road • Water did not flood the maneaba (in figure above) – inundation depth <20 cm 	<ul style="list-style-type: none"> • Water crossed the road in (B) • In front of the maneaba (A), inundation depth ranges from 5 cm to 12 cm

Table 6. Comparison between observed and simulated inundation at location 5.


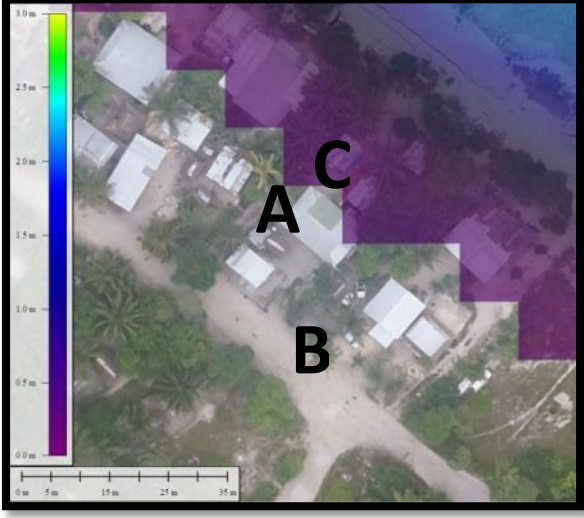

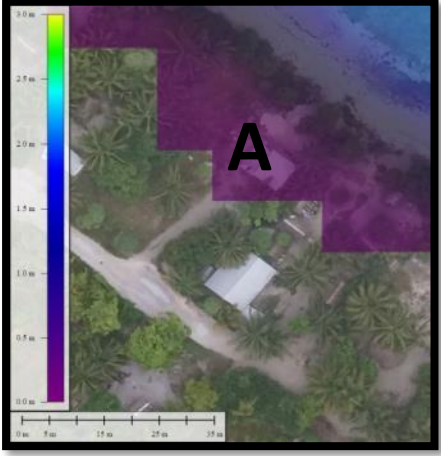
Location 5	Observed	Modelled
Image		
Details	<ul style="list-style-type: none"> • Water reached the well but did not overtop the bricks • Sea water almost reached the road (B) • Inundation depth at the well <20 cm 	<ul style="list-style-type: none"> • Inundation stopped 4 m before the well (A) • Inundation stopped 18 m from the road (B) • Inundation depth near the well is 19 cm

Table 7. Comparison between observed and simulated inundation at location 6.

Location 6	Observed	Modelled
<p>Image</p>		
<p>Details</p>	<ul style="list-style-type: none"> Water reached the house shown in the image, but the water depth was <10–15 cm and did not inundate the house 	<ul style="list-style-type: none"> Inundation reached the house (A); inundation depth in front of the house is between 5 cm and 8 cm

Inundation extent is in good agreement with information collected at locations 1, 2, 4 and 6.

Noticeable discrepancies are seen in locations 3 and 5, where the model simulates a smaller inundation extent. Poor baseline data around location 3 can explain the relatively small simulated inundation extent compared with the observed inundation.

At location 5, modelled inundation depth is in good agreement with the observed inundation. However, inundation does not extend as far as it has been described by witness accounts. This discrepancy can be attributed to poor baseline data. Although good-quality topography data were collected from the RTK GPS, data are very sparse between the beach and the road. In contrast, the unmanned aircraft vehicle data offer an almost total coverage of the area, but where land coverage is complex (e.g. between houses and trees) accuracy is low when flying at high altitude.

7. Results

The validation exercise established confidence in the model, and it was deemed appropriate to use it to investigate the potential inundation generated from 72 possible events (BIVA severe and extreme scenarios report): 36 scenarios characterised by a storm tide level and a wave height on each side of Bonriki – the lagoon side and the ocean side.

A probability (20-year RI, 50-year RI and 100-year RI) and a climate change scenario are attributed to each scenario. Four SLR scenarios were considered: today’s sea level, RCP6.0 and RCP8.5 from the Fifth Assessment Report of the Intergovernmental Panel on Climate Change, and the intermediate–high scenario from Parris et al. (2012) (BIVA severe and extreme scenarios report). In this study, we used the SLR projections for 2064 (50 years from now) for each climate change scenarios as determined in the BIVA development of scenario report (Table 8).

Table 8. 2064 Sea level rise (SLR) projections for Tarawa.

2064 SLR under RCP6.0	2064 SLR under RCP8.5	2064 intermediate–high SLR
0.22 m	0.28 cm	0.49cm

Each model run simulates one hour of sea-state condition (after a model warm-up period) with a wave group following a JONSWAP spectrum. Model output is processed into a map of maximum inundation depth.

7.1. Impact groups

The scenarios were then distributed into five impact groups, depending on the inundation extent and the potential impact on the groundwater lens.

- **Minor A:** Minor inundation with no impact on groundwater (A). Inundation extent is contained near the shoreline, from 10 m to 30 m inland. A representative map for offshore and lagoon conditions can be seen in Figure 28 and Figure 29.
- **Minor B:** Minor inundation with no impact on groundwater (B). Inundation contained to the coastal fringes of the islet but extends further than minor A, with sea water reaching as far as the coastal road in places, thereby representing a significant impact on the built environment and coastal communities. A representative map for offshore and lagoon condition can be seen in (Figure 30 & Figure 30).
- **Moderate:** Moderate inundation with minor impact on groundwater. This group of scenarios represents a relatively significant inundation extent, reaching deeper inside the islet in places. Sea water reaches the groundwater infrastructure (galleries and pumps), which poses a potential risk to the groundwater resource. A representative map for offshore and lagoon condition can be seen in (Figure 32 & Figure 33).
- **Severe:** Severe inundation with moderate impact on groundwater. From the ocean side, inundation extent reaches the central part of the Islet, but does not cross the islet, affecting numerous freshwater galleries. Ocean scenarios lead to a significant overtopping of the road on the western side. Lagoon scenarios show saltwater intrusion into the saltwater marsh. A representative map for offshore and lagoon condition can be seen in (Figure 34 & Figure 35).
- **Extreme:** Extreme inundation with significant impact on groundwater. Inundation extent goes from the oceanic shore to the lagoon, across the islet. Inundation extent also reaches the

runway. At least half of the freshwater galleries are within the inundated area. A representative map for offshore and lagoon condition can be seen in (Figure 36 & Figure 37).

About 50 % of the scenarios are grouped into the minor A and minor B groups – 49% of the offshore scenarios and 50% of the lagoon scenarios. The moderate impact group represents 23% of the offshore scenarios and 17% of the lagoon scenarios. The severe impact group represents 17% of the offshore scenarios and 25% of the lagoon scenarios. Finally, 11% of the offshore scenarios and 8% of the lagoon scenarios are considered as extreme. The distribution of the scenarios into impact groups can be seen in (Figure 38 and Figure 39).

The scenarios are well distributed into the different impact groups. Half of the 72 inundation scenarios show only a minor inundation, with inundation contained near the shoreline. Although those scenarios are expected to have no impact on the groundwater resource, they still pose a direct threat to people living near the shore. Additionally, the high percentage of scenarios contained in the moderate and severe impact groups highlights the relevance of this probabilistic study and justifies concerns on the potential vulnerability of the groundwater resource. Finally, while the extreme impact group is smaller, it cannot be taken as a marginal impact because it contains a significant number of scenarios (four ocean scenarios and three lagoon scenarios).

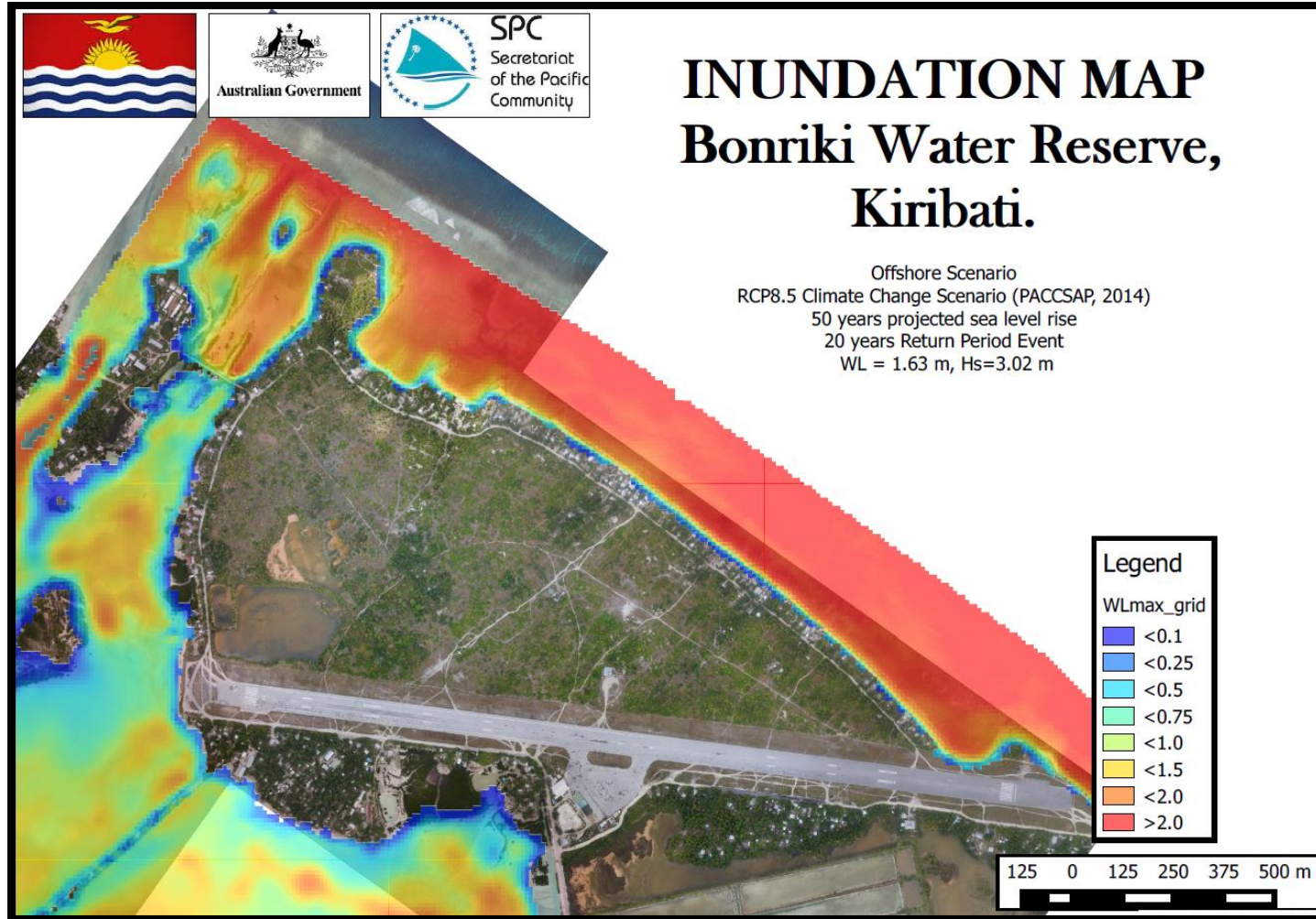


Figure 28. Offshore representative inundation map – minor A.

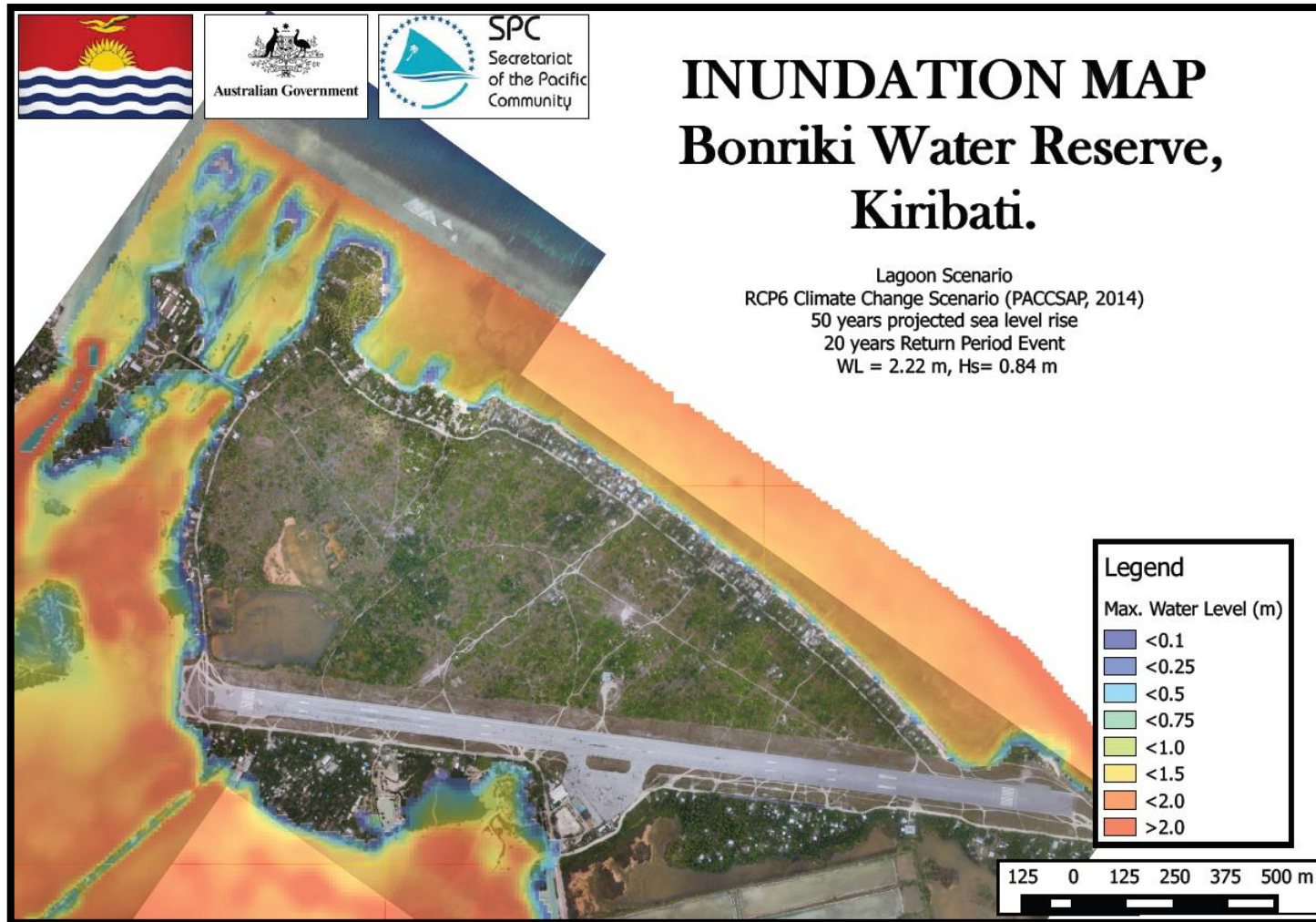


Figure 29. Lagoon representative inundation map – minor A.

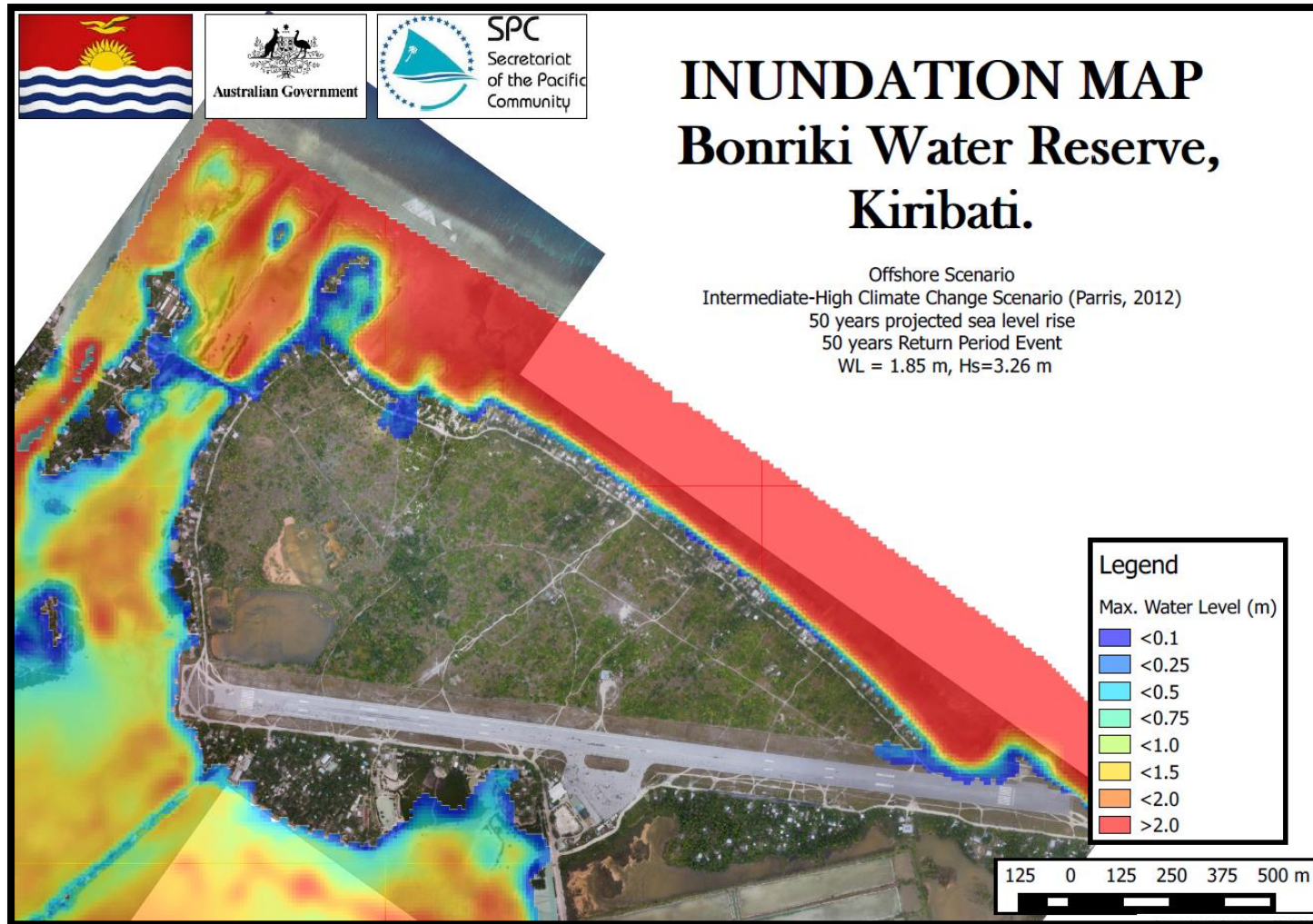


Figure 30. Offshore representative inundation map – minor B.

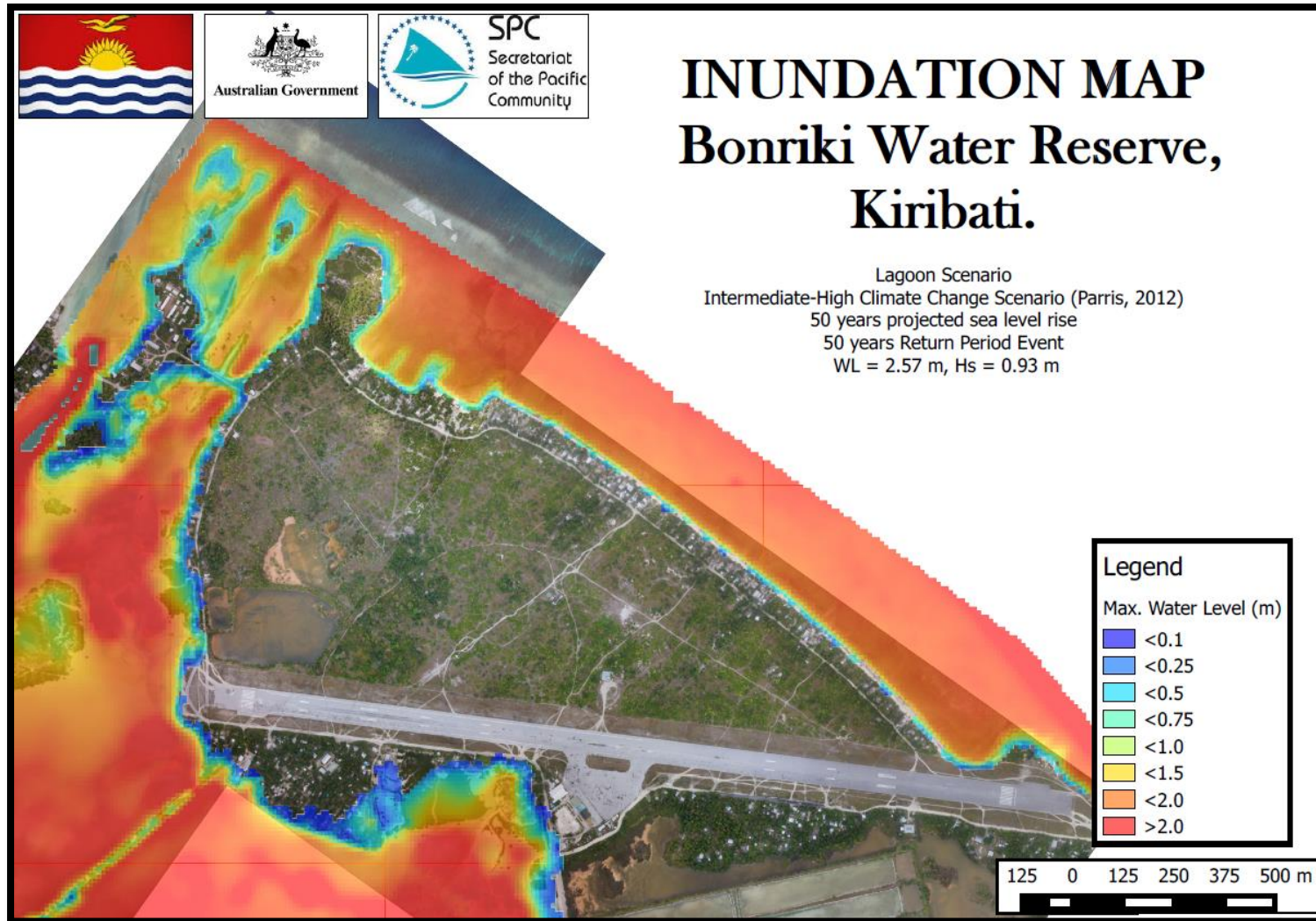


Figure 31. Lagoon representative inundation map – minor B.

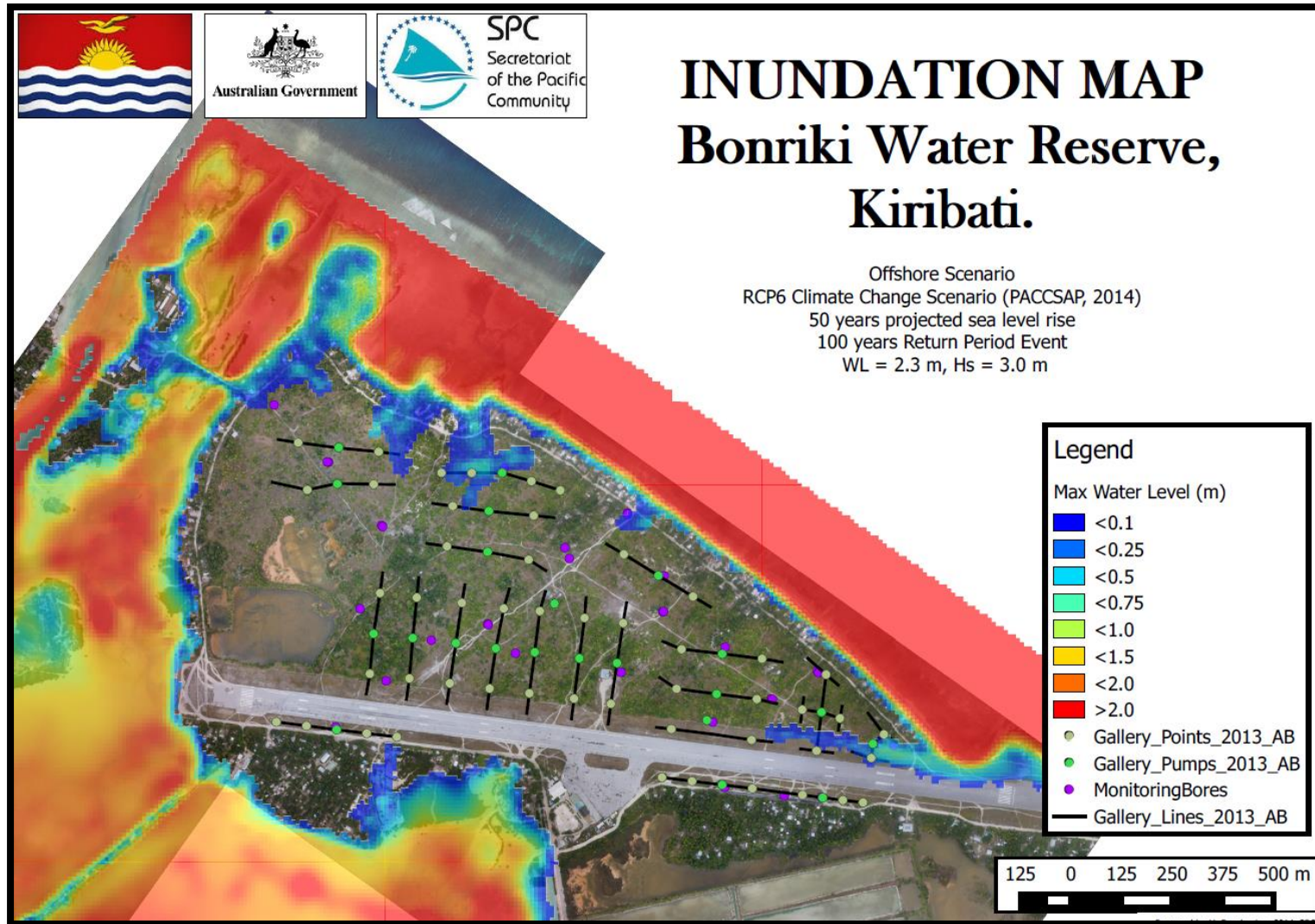


Figure 32. Offshore representative inundation map – moderate.

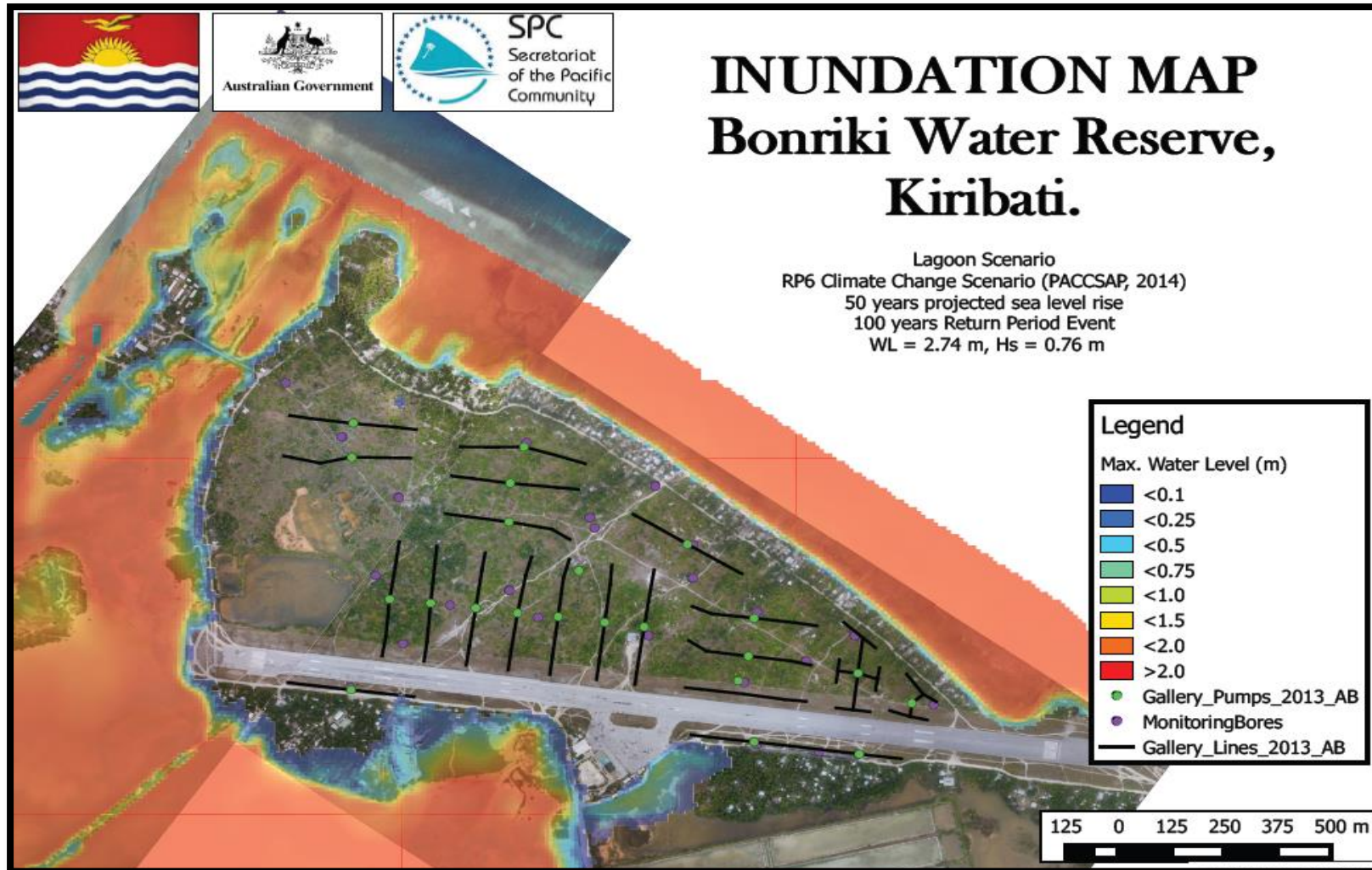


Figure 33. Lagoon representative inundation map – moderate.

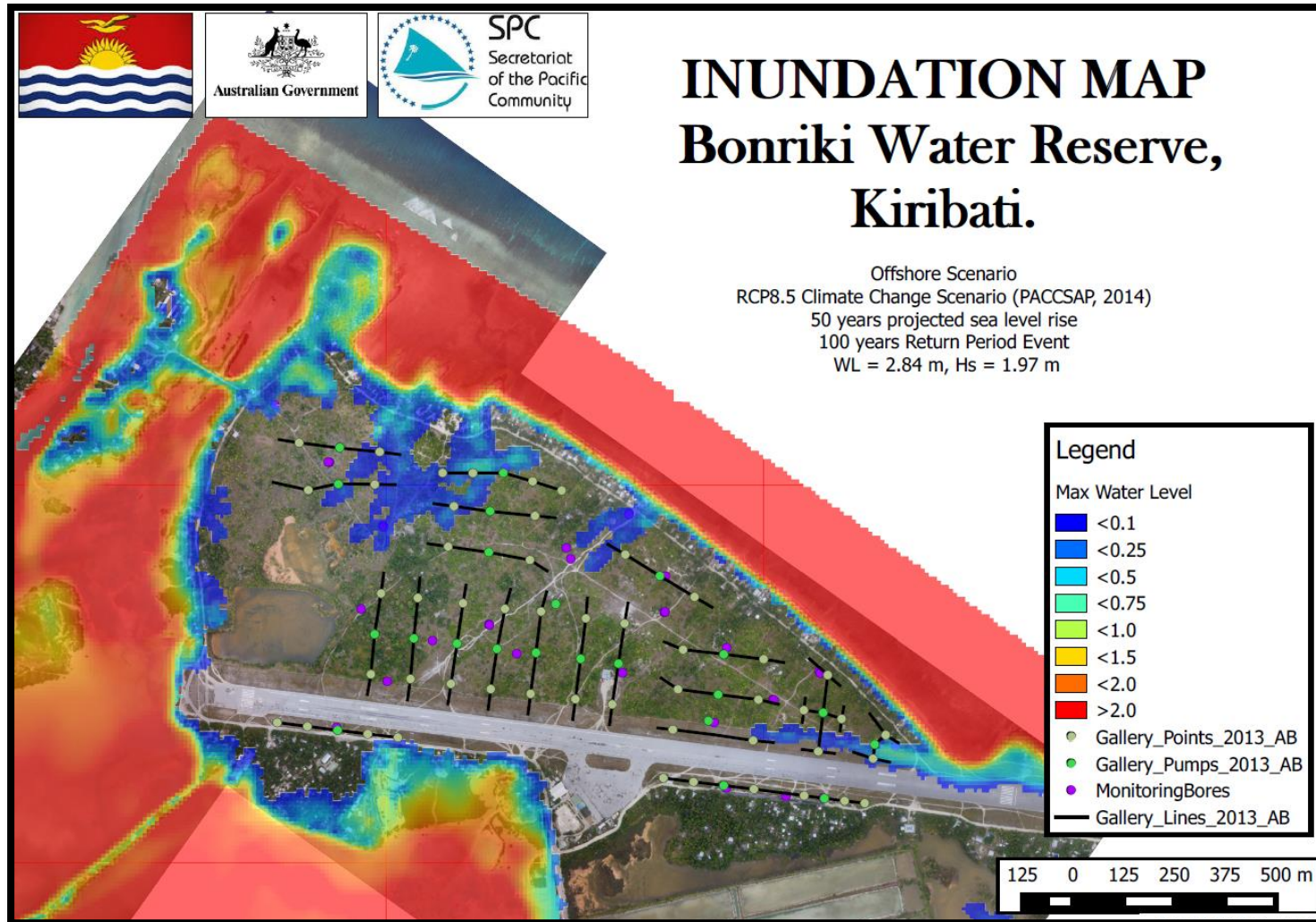


Figure 34. Offshore representative inundation map – severe.

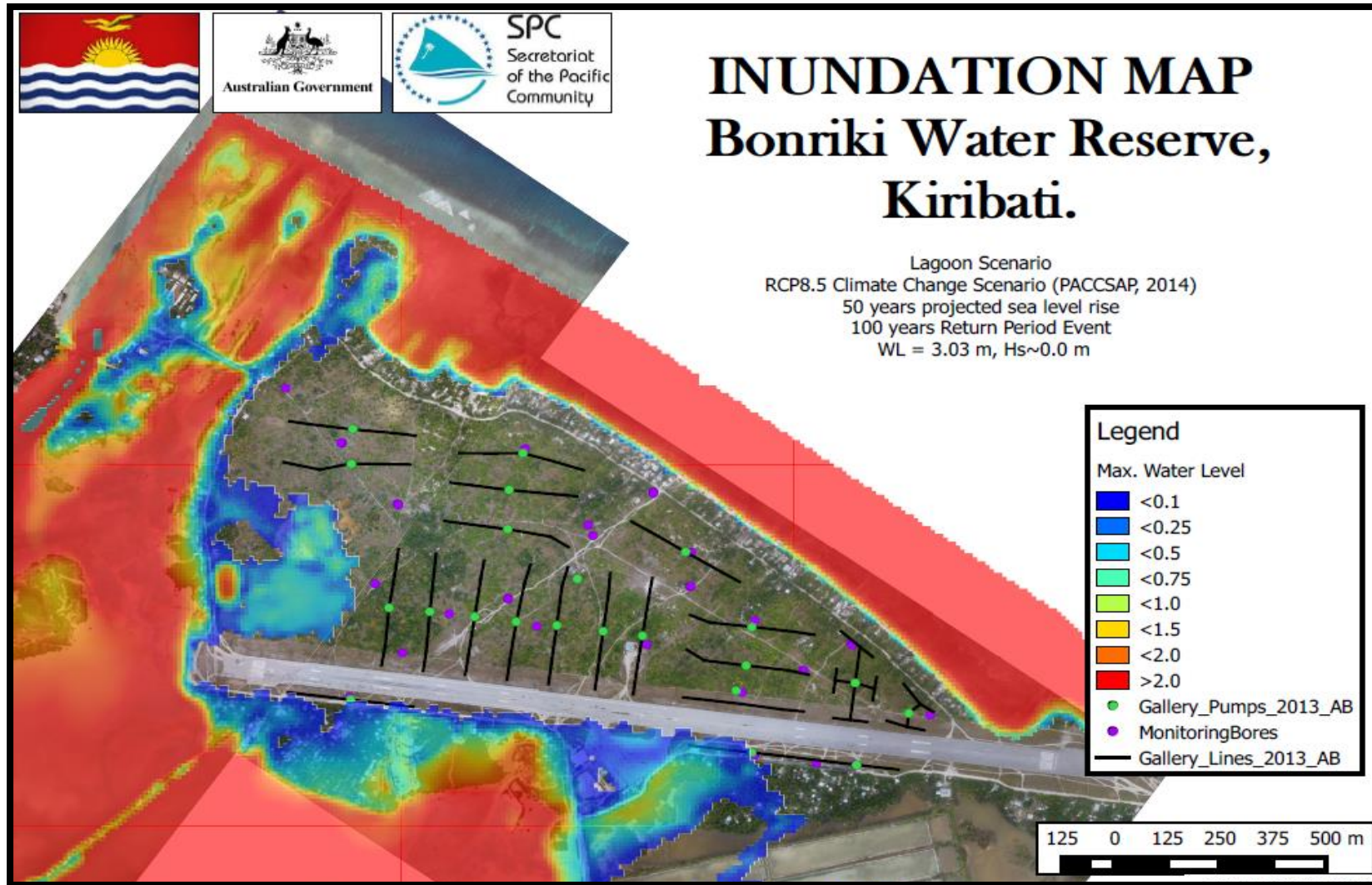


Figure 35. Lagoon representative inundation map – severe.

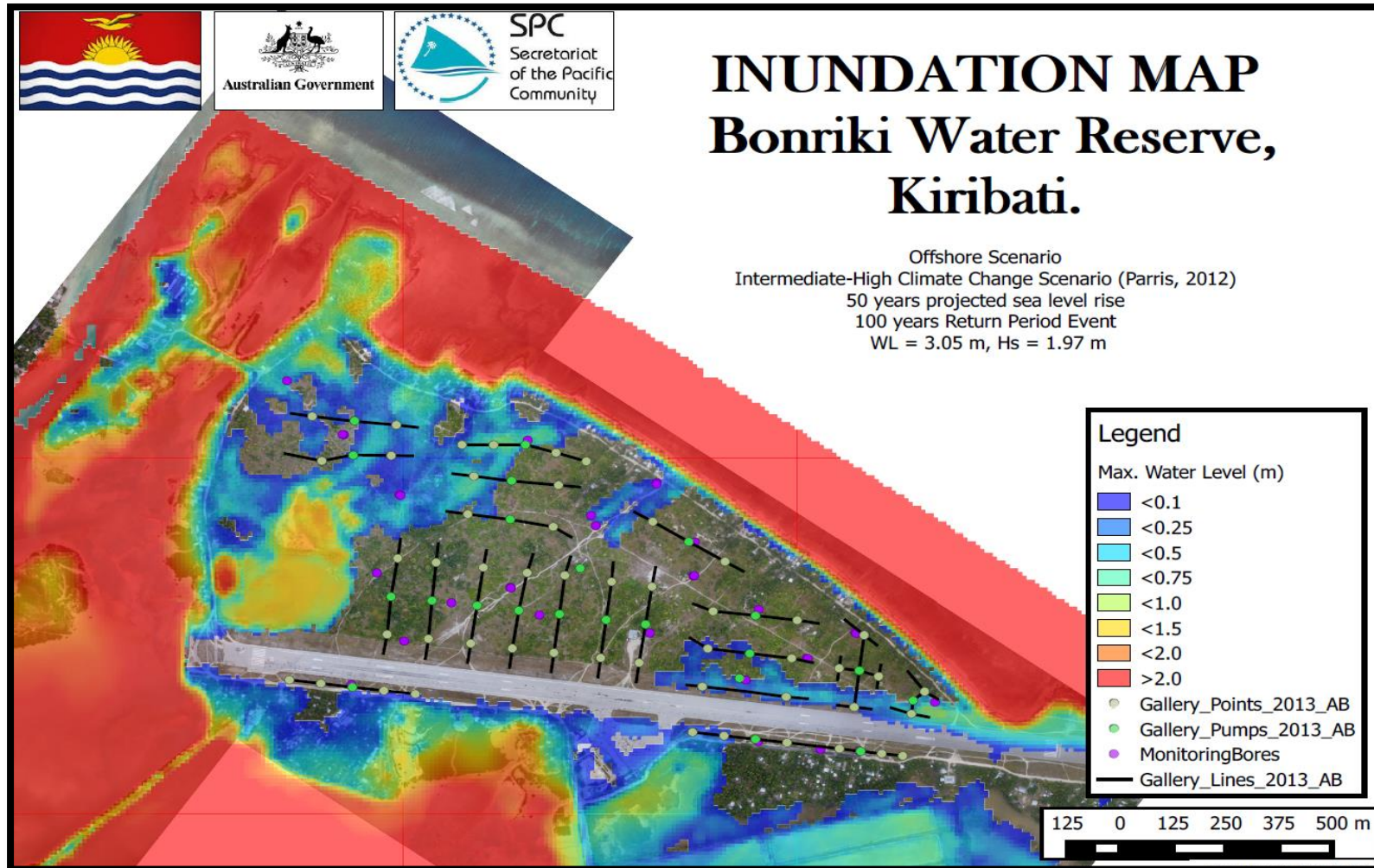


Figure 36. Offshore representative inundation map – extreme.

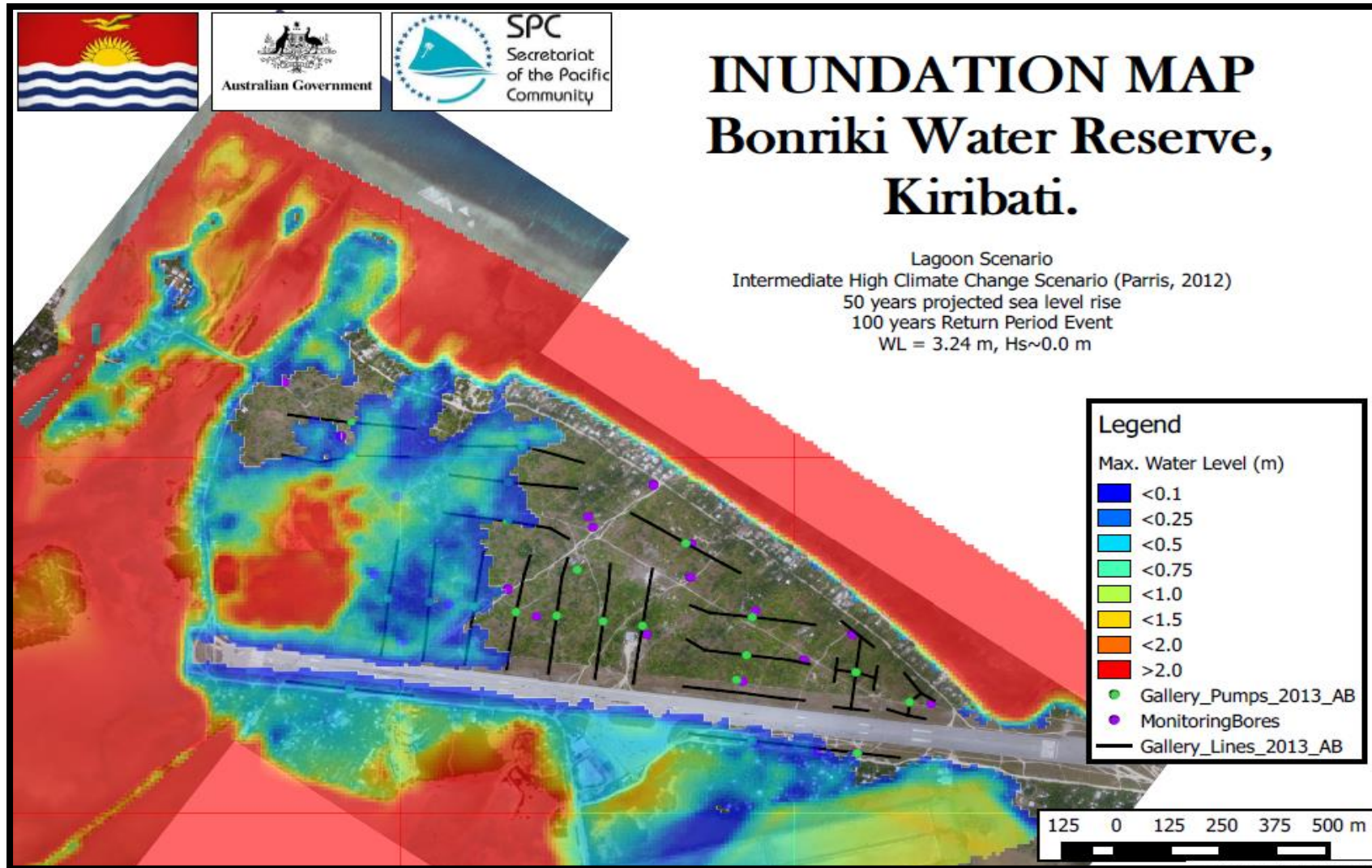


Figure 37. Lagoon representative inundation map – extreme.

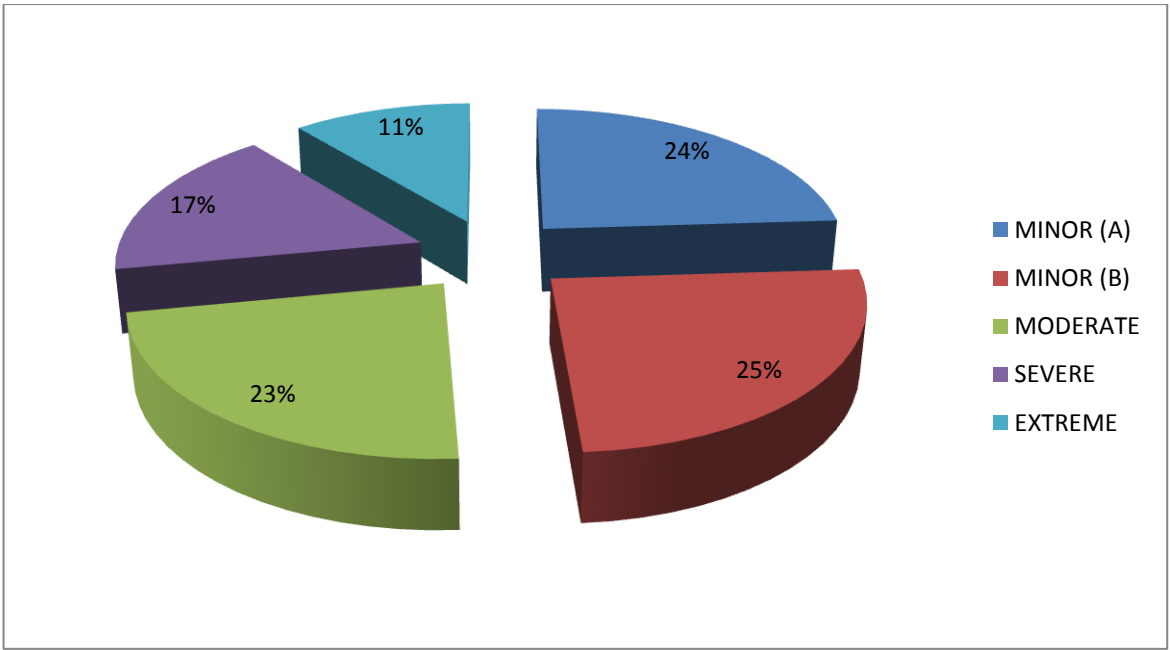


Figure 38. Distribution of the offshore scenarios into risk groups.

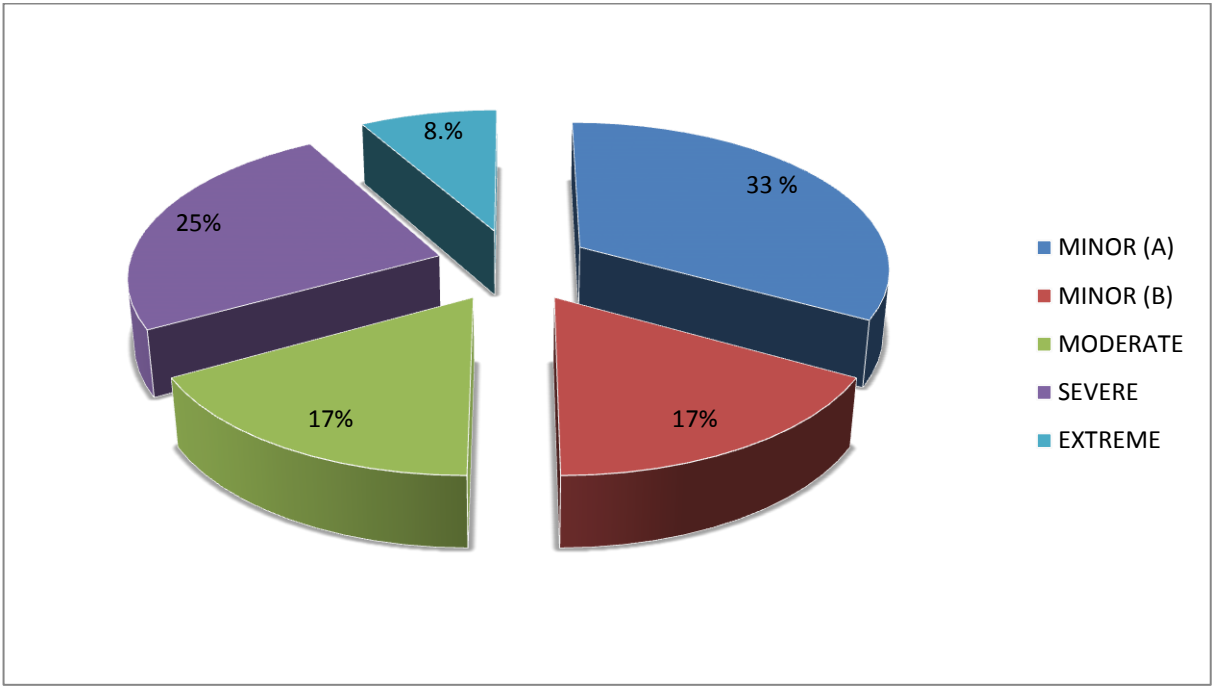


Figure 39. Distribution of the lagoon scenarios into risk groups.

7.2. Impact of sea level rise

Interesting findings can be reached by looking at the distribution of SLR scenarios in the different impact groups (Figure 40). Of the 18 scenarios built with the present day sea level, all but one scenario groups in the minor A and minor B impact categories. This result highlights the current low exposure of the Bonriki groundwater reserve to saltwater intrusion. It is well in line with the 3 March event, ranked as a 100-year RI, which would be categorised into the minor B impact group. This finding also highlights the potential exacerbation of the inundation hazard due to the projected SLR.

Furthermore, all scenarios generating extreme impacts are built with the intermediate–high SLR scenario from Parris et al. (2012). It represents the upper limit of SLR projection considered in this study, with a 49 cm SLR in 2064. This SLR scenario is also currently considered as the least likely to occur.

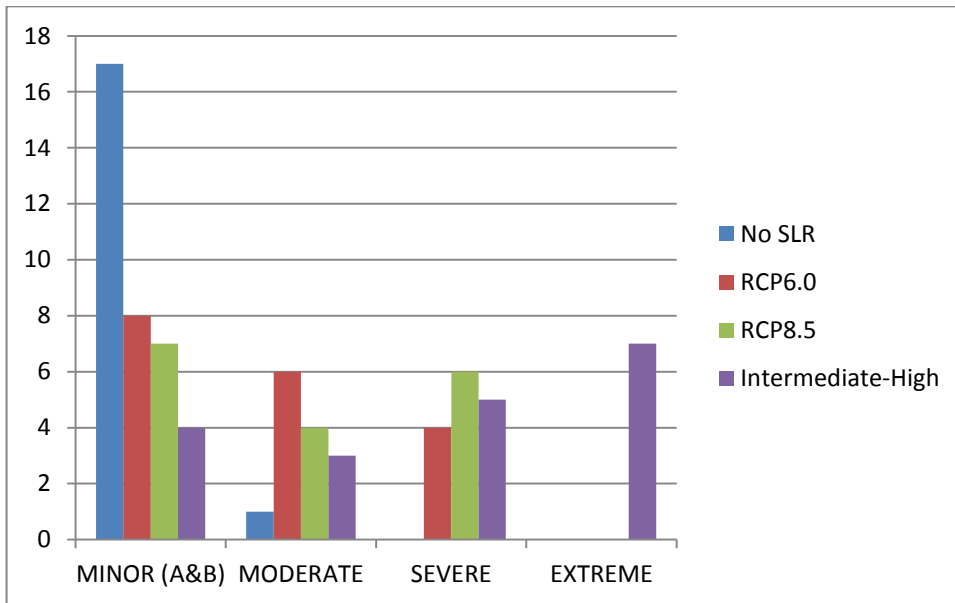


Figure 40. Distribution of the scenarios into impact groups, depending on their attributed SLR projection.

7.3. Shoreline vulnerability and inundation pathways

This study highlighted several inundation pathways along the coast. Finding such weak points is a first step to developing options to reduce the effects of inundation.

The shoreline can be roughly divided into three categories depending on its current vulnerability towards land submersion (Figure 41).

- Vulnerability 1: Only minor inundation is generated across the coastline throughout all scenarios.
- Vulnerability 2: Significant submersion of the coastline, potentially triggering impact on the freshwater lens, only occurs during severe and extreme scenarios as described above. However, minor inundation can be triggered with lower impact.
- Vulnerability 3: Parts of the shoreline that represent the preferred inundation pathways into Bonriki islet even under current sea level. Significant submersion of the coastline, potentially triggering impact on the freshwater lens, occurs from a moderate scenario and above. All scenarios showed this category of shoreline to be prone to inundation, and all parts of the coastline in this category were reported as flooded after the March 2014 event.

The airport runway does not get significantly flooded in any of the 72 scenarios.

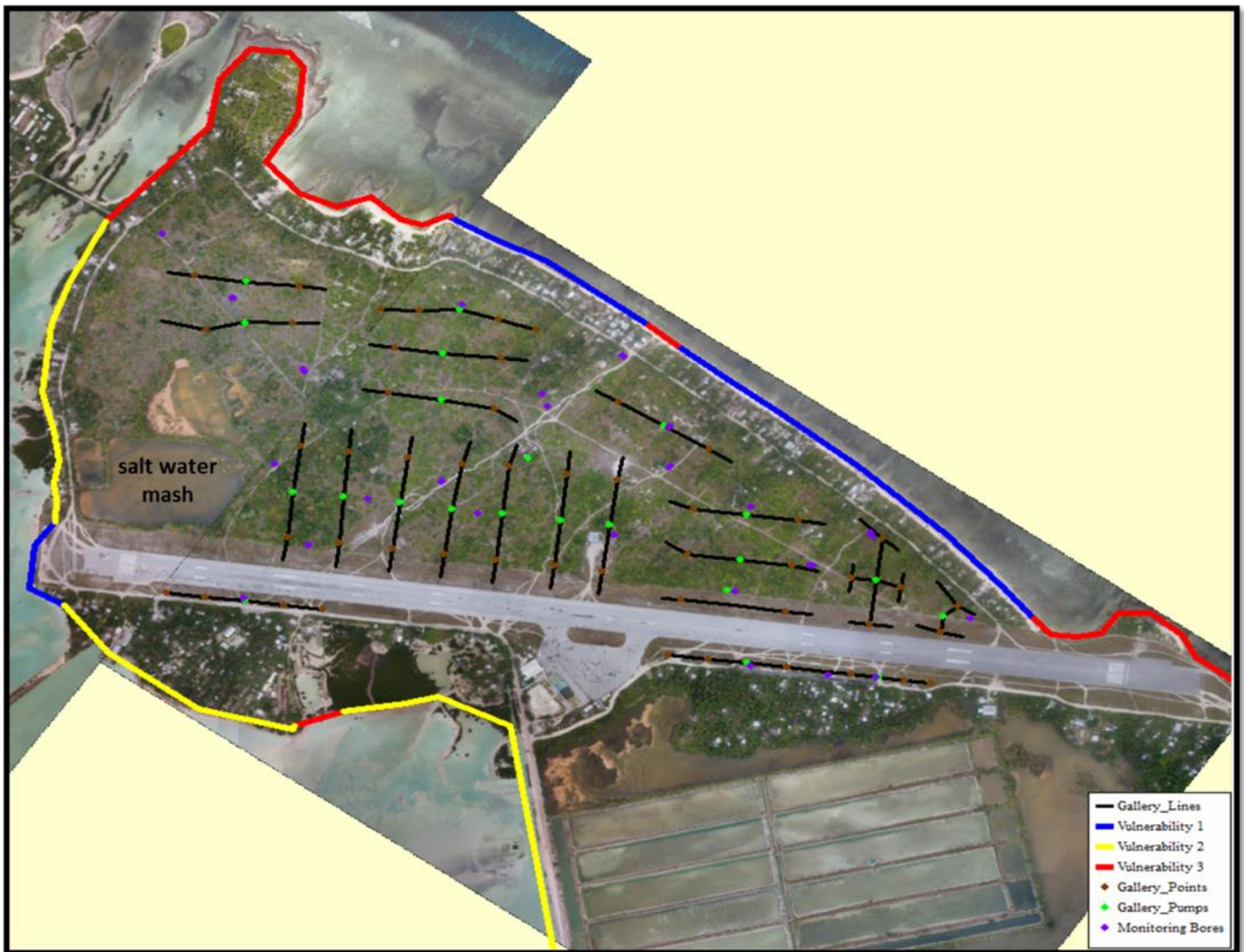


Figure 41. Coastline vulnerability to inundation event.

The potential erosion inherent from the impact of the 72 scenarios is not taken into account in this study. However, during an inundation event, land overtopping can cause the lowering of the beach berm and in turn could drastically increase the vulnerability of the ocean coastline. Additionally, the parts of the coastline on the ocean side that are categorised as having low vulnerability (vulnerability 1) have been eroding significantly since 1984, as seen in the BIVA coastal change analysis report. Average erosion has been at a rate of 0.6 m/year, with a maximum erosion rate of more than 1 m/year (Figure 42). This erosion trend is worsened by ad hoc seawalls along the shoreline, as shown by the evidence collected during a shoreline mapping survey undertaken in August 2014 as part of this project (BIVA shoreline change analysis report and Figure 43).

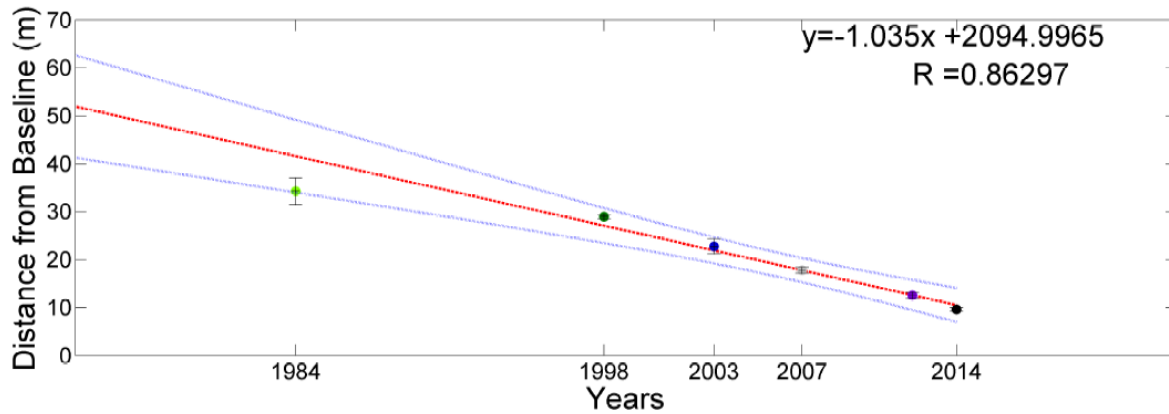


Figure 42. Weighted linear regressions, showing erosion since 1984 at transect 9 (Source: BIVA shoreline change analysis report).



Figure 43. Photo showing erosion scar (>50 cm) on the ocean side of Bonriki.

The north western coastline, on the ocean side, currently categorised as highly vulnerable (vulnerability 3), is shown to be a primary inundation pathway, in part because of its low beach berm. The shoreline change analysis study, undertaken as part of this project (BIVA shoreline change analysis report) shows this coastline to be undergoing accretion (2.5 m/year) trend since 1943 (Figure 44). Although the accretion rate has significantly decreased in recent years, since 1998 accretion has been consistent (R = 0.96) and rapid (0.78 m/year) (Figure 45). This fast and consistent change on that shoreline could lead to a significant reduction of the inundation hazard in the near future, if the natural shoreline environment is managed appropriately.

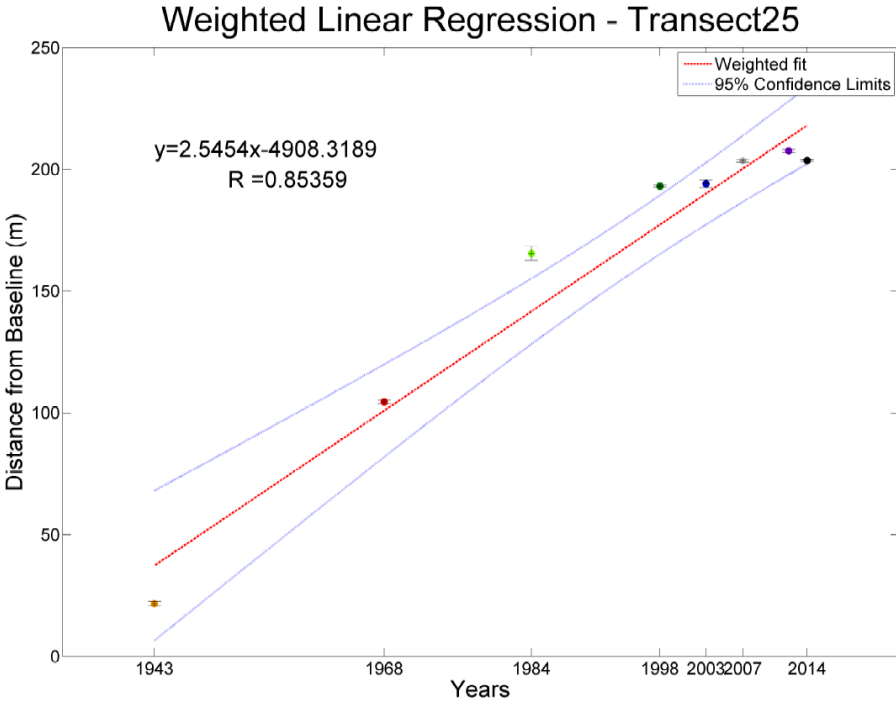


Figure 44. Weighted linear regressions showing accretion since 1943 at transect 25 (Source: BIVA shoreline change analysis report).

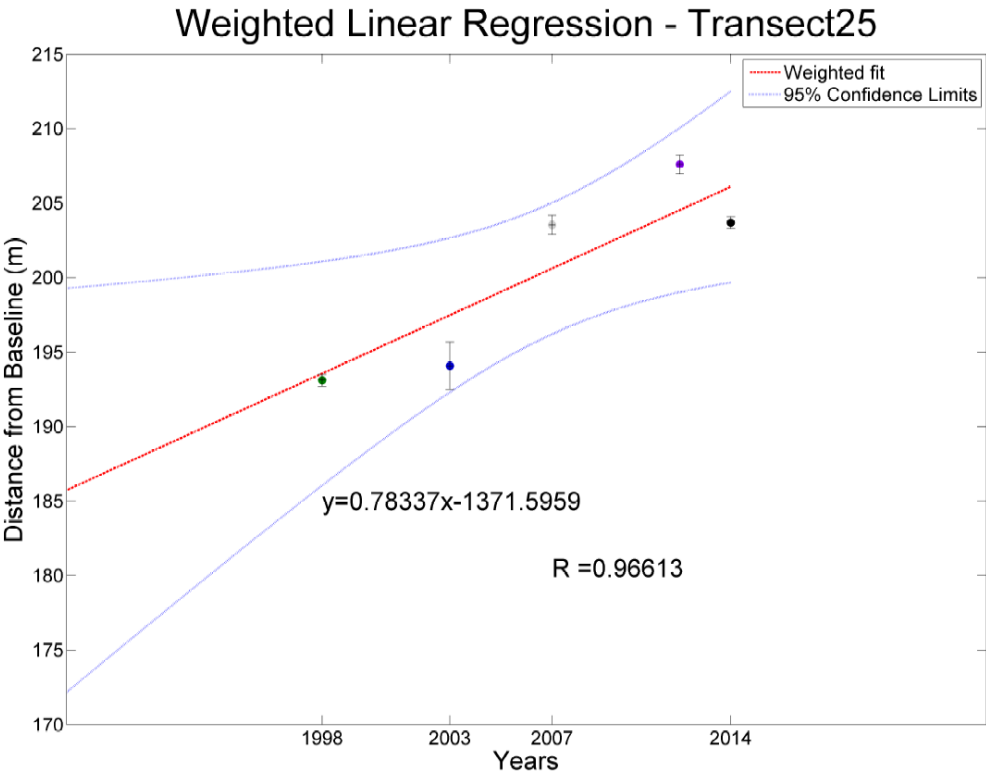


Figure 45. Weighted linear regressions showing accretion since 1998 at transect 25 (Source: BIVA shoreline change analysis report).

Emphasis should also be put on the coastline seaward of the saltwater marsh on the western coastline of Bonriki. Currently, the road that separates the lagoon and the saltwater marsh is relatively high (3 m above tide gauge zero, the vertical reference point) and reduces the frequency of overtopping of the landward area. However, if overtopping does occur it can lead to a potentially salinization of the freshwater lens as saltwater flows into the saltwater marsh, which has relatively low salinity levels. It is recommended that this area is monitored.

7.4. Storm tide versus wave height, the dominant contributor to inundation

The scenarios were developed based on the joint probability curves between storm tide and water level generated for Bonriki (BIVA report on severe and extreme scenarios), where storm tide is an elevated water level with contributions from the tide, storm surge and the mean level of the sea. For each curve, representing a 20-, 50- or 100-year RI, three scenarios were chosen to characterise a storm tide level and a wave height, as follows:

- A high wave condition: High wave height with low storm tide level.
- A mix of conditions: Medium wave height and storm tide level.
- A high storm tide condition: Low wave height and high storm tide level.

High and low are relative to a RI in all scenarios.

The distribution of these three categories into the five impact groups was investigated for the offshore and lagoon scenarios (Figure 46 and Figure 47).

Results show that for events with the same RI, those characterised with a high storm tide lead to greater impacts. In other words, storm tide is a greater contributor to coastal inundation than wave height. On the lagoon side, with only small wave heights being considered (up to $H_s = 1.0$ m for a 100-year RI), such results can be expected. However, on the ocean side, with H_s ranging from 2.0 m to 3.43 m, this result is less obvious. Two main reasons can be put forward to explain the stronger contribution from the storm tide to the inundation.

- The lower the water level on the reef, the more the wave energy dissipates through bottom friction. With a high water level on the reef flat due to storm tide, waves experience less dissipation and are more likely to reach the shore. The influence of tidal level on the dissipation of the infragravity wave can be clearly seen from the oceanographic data collected (Figure 8).
- A field study in Ipan Reef, Guam, showed a greater potential for resonance of the infragravity waves on the reef flat as water level rises (Péquinet et al. 2009).

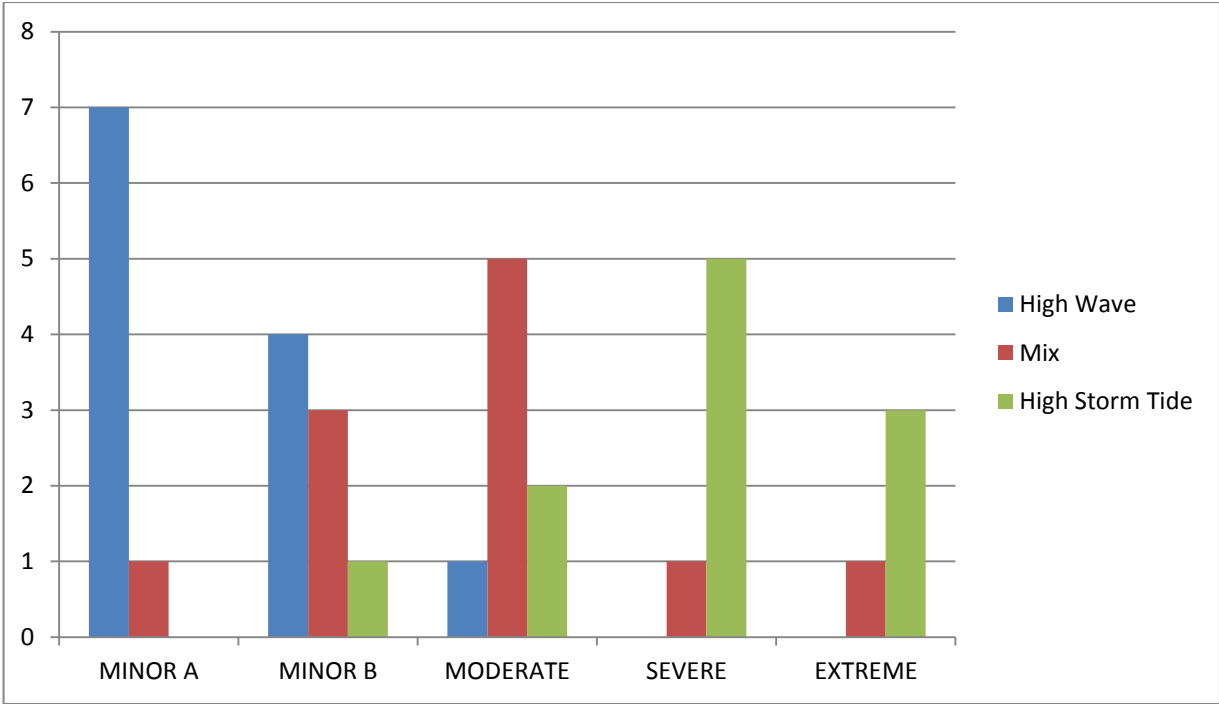


Figure 46. Offshore side – distribution of the scenarios into impact groups depending on their dominant component; either a high storm tide, a high wave height or a mix of both.

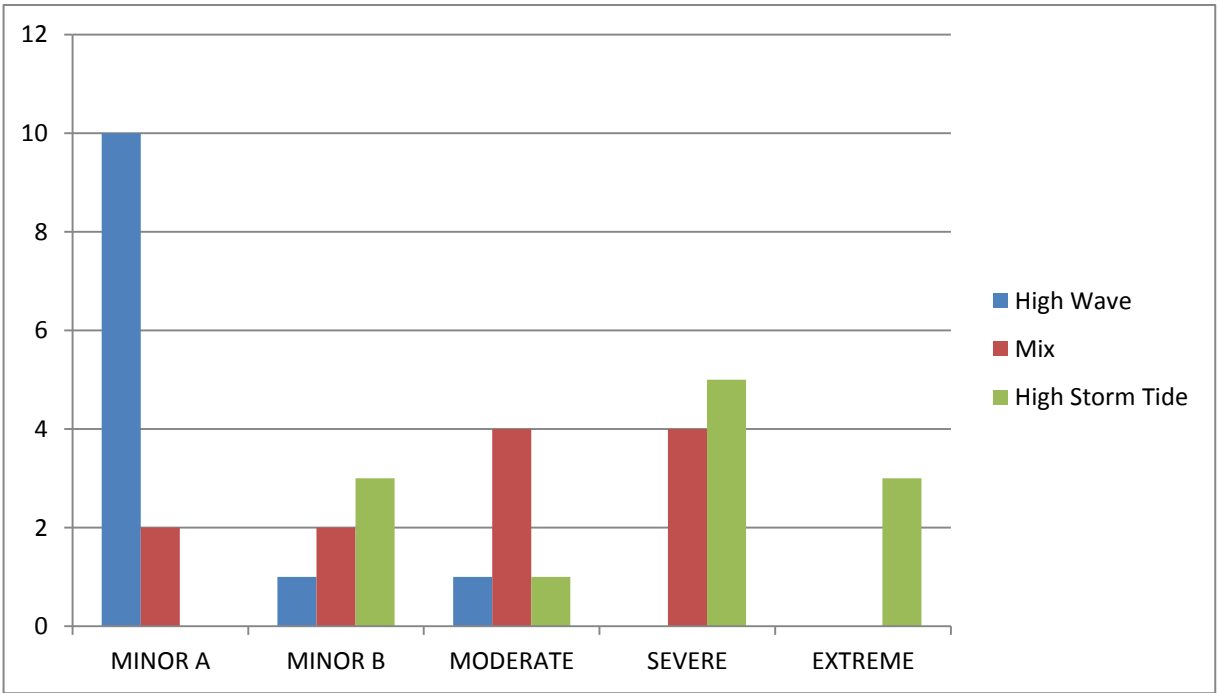


Figure 47. Lagoon-side – distribution of the scenarios into impact groups depending on their dominant component; either a high storm tide, a high wave height or a mix of both.

8. Conclusion

This report describes the last piece of the Bonriki probabilistic inundation hazard assessment study. It combines outcomes from five reports: topography, bathymetry, oceanography, scenario and coastline change analysis.

The XBeach model was thoroughly validated against on-the-ground observations from the March 2014 inundation event. With confidence in the ability of the model to simulate realistic inundation impacts on Bonriki, it was used to generate inundation maps from 72 probable scenarios. Those scenarios are developed based on a statistical analysis of the historical wave and water-level data generated around Bonriki. The inclusion of three SLR scenarios allowed the impact of climate change on the Bonriki inundation hazard to be investigated.

The study made some key findings.

- Currently, the risk of significant inundation of Bonriki leading to potential impact on the groundwater is low. All but one scenario developed with today's sea level shows minor inundation, similar to the March 2014 event. Although the inundation is confined to the shoreline, it poses a significant threat to the coastal community that predominantly settle along the coastal fringe.
- Sea level rise significantly exacerbates the risk of inundation. The two likely emission scenarios – RCP6.0 and RCP8.5 – increase the inundation impact to moderate and severe, respectively. Only scenarios built with the intermediate–high scenario of Parris et al., lead to extreme inundation potentially generating significant impact on the freshwater lens.
- Several dominant inundation pathways have been highlighted in the study. Certain parts of the Bonriki coastline are relatively susceptible to overtopping and inundation during extratropical storm events that develop in the northern Pacific and/or by high storm tides. The boreholes pumps and galleries in close proximity to these areas are at increased risk to saltwater incursion.
- Rapid and consistent changes in parts of the Bonriki shoreline as a result of erosion and accretion mean that inundation pathways and, more generally, inundation hazards can change in the near future. The resilience of the shoreline and risk to local communities could be reduced by developing and implementing an integrated coastal zone management (ICZM) plan. The results of the BIVA project would provide an excellent baseline for an ICZM plan.

This study did not investigate in detail the possibility and aftermath of the resonance of the infragravity wave on the reef flat. A field study on Ipan Reef in Guam showed a greater potential for the resonance of infragravity waves on the reef flat as water level rises (Péquinet et al. 2009). Under similar conditions to this study ($H_s = 4$ m, water level on the reef flat of 2 m and reef flat length of 450 m), a near resonance of the far infragravity wave was demonstrated following the modes of a bounded open basin. Such resonance would significantly increase the amount of energy at the shoreline. Although no specific processing was undertaken to study the potential resonance of the infragravity waves at Bonriki, it is accounted for by the XBeach model, and in turn is reflected in the outcome of this inundation hazard study. The resonance of the infragravity wave could explain the significant contribution of SLR to the inundation impact highlighted in this study.

9. References

- Andrews D.G. and McIntyre M.E. 1978. An exact theory of nonlinear waves on a Lagrangian-mean flow. *Journal of Fluid Mechanics* 89(4):609–646.
- Begg Z., Damlamian H., Raj A., Lal A. and Krüger J. 2015. *Bonriki inundation vulnerability assessment project topography survey*. Kiribati Bonriki, Tarawa, Kiribati. Report for Bonriki Inundation Vulnerability Assessment Project. Geoscience Division Secretariat of the Pacific Community. SPC report SPC00003.
- Brander R.W., Kench P.S. and Hart D. 2004. Spatial and temporal variations in wave characteristics across a reef platform, Warraber Island, Torres Strait, Australia. *Marine Geology*, 207(1):169–184.
- Damlamian, H., Kruger, J., Turagabeci, M. and Kumar, S. 2013. Cyclone wave inundation models for Apataki, Arutua, Kauehi, Manihui and Rangiroa Atolls, French Polynesia. SPC GSD Technical Report PR176.
- Damlamian H., Bosserelle C., Kruger J., Raj A., Begg Z. and Kumar S. 2015a. *Development of severe and extreme scenarios of wave and water level through statistical analysis and numerical modelling in Bonriki, Tarawa, Kiribati*. Report for Bonriki Inundation Vulnerability Assessment Project. Geoscience Division Secretariat of the Pacific Community. SPC Report SPC00002.
- Dean R.G. and Dalrymple R.A. 2002. *Coastal processes with engineering applications*. New York: Cambridge University Press.
- Dean R.G. and Dalrymple R.A. 1991. *Water wave mechanics for engineers and scientists*.
- KNSO and SPC 2012. Kiribati 2010 census. Volume 2, Analytical report. Kiribati National Statistics Office and the Secretariat of the Pacific Community Statistics for Development Program
- Kruger, J., and Sharma, A., 2008. High-resolution bathymetry survey of Kiribati. SOPAC Technical Report 114.
- Kumar S. 2015 *Single beam survey*. Report for Bonriki Inundation Vulnerability Assessment Project. Geoscience Division Secretariat of the Pacific Community, SPC Report SPC00004.
- Longuet-Higgins, M.S. and Stewart R.W. 1962. Radiation stress and mass transport in gravity waves, with application to 'surf beats'. *Journal of Fluid Mechanics* 13(4):481–504.
- Lowe R.J., Falter J.L., Bandet M.D., Pawlak G., Atkinson M.J., Monismith S.G. and Koseff J.R. 2005. Spectral wave dissipation over a barrier reef. *Journal of Geophysical Research: Oceans* (1978–2012): 110(C4).
- Lowe R.J., Falter J.L., Monismith S.G. and Atkinson M.J. 2009. Wave-driven circulation of a coastal reef–lagoon system. *Journal of Physical Oceanography* 39:873–893.

Lugo-Fernandez A., Roberts H.H., Wiseman Jr W.J. and Carter B.L. 1998. Water level and currents of tidal and infragravity periods at Tague Reef, St. Croix (USVI). *Coral Reefs* 17(4):343–349.

Parris, A., P. Bromirski, V. Burkett, D. Cayan, M. Culver, J. Hall, R. Horton, K. Knuuti, R. Moss, J. Obeysekera, A. Sallenger, and J. Weiss, 2012. *Global Sea Level Rise Scenarios for the US National Climate Assessment*. NOAA Tech Memo OAR CPO-1. 37 pp.

Péquignet A.C.N., Becker J.M., Merrifield M.A. and Aucan J. 2009. Forcing of resonant modes on a fringing reef during tropical storm Man-Yi. *Geophysical Research Letters* 36(3).

Raj A., Damlamian H. and Kruger J. 2015b *Shoreline change analysis*. Report for Bonriki Inundation Vulnerability Assessment Project. Geoscience Division Secretariat of the Pacific Community. SPC Report SPC00006.

Pomeroy, A., Lowe, R.J., Symonds, G., van Dongeren, A., Moore, C., 2012. The dynamics of infragravity wave transformation over a fringing reef. *Journal of Geophysical Research – Oceans*, 117, C11022.

Reniers A.J., Roelvink J.A. and Thornton E.B., 2004. Morphodynamic modeling of an embayed beach under wave group forcing. *Journal of Geophysical Research* 109(C1):C01030.

Roelvink D., Reniers A., van Dongeren A., van Thiel de Vries J. and McCall R. 2010. *XBeach model description and manual*. The Netherlands: Unesco-IHE Institute for Water Education and Delft: Deltares and Delft University of Technology, p. 108.

Roelvink J.A. and Brøker I. 1993. Cross-shore profile models. *Coastal Engineering* 21(1):163–191.

Sánchez, A., Smith, J.M., Demirbilek, Z, Boc, S. (2007) *User’s manual to the Coastal Modeling Package – TWAVE*, Unpublished Letter Report, Vicksburg, MS, U.S. Army Engineer and Research Development Center.

Symonds G., Huntley D.A. and Bowen A.J. 1982. Two-dimensional surf beat: Long wave generation by a time-varying breakpoint. *Journal of Geophysical Research: Oceans (1978–2012)* 87(C1):492–498.

Taebi S., Lowe R.J., Pattiaratchi C.B., Ivey G.N., Symonds G. and Brinkman R. 2011. Nearshore circulation in a tropical fringing reef system. *Journal of Geophysical Research: Oceans (1978–2012)* 116(C2).

Young I.R. 1989. Wave transformation over coral reefs. *Journal of Geophysical Research: Oceans (1978–2012)* 94(C7):9779–9789.

Bureau of Meteorology. (2010). *Pacific Country Report, Sea Level & Climate*. Kiribati. South Pacific Sea Level and Climate Monitoring Project.

Pomeroy, A., Lowe, R., Symonds, G., Van Dongeren, A. and Moore, C., 2012. The dynamics of infragravity wave transformation over fringing reef. *Journal of Geophysical Research-Oceans*, 117.



CONTACT DETAILS
Secretariat of the Pacific Community

SPC Headquarters
BP D5,
98848 Noumea Cedex,
New Caledonia
Telephone: +687 26 20 00
Fax: +687 26 38 18

SPC Suva Regional Office
Private Mail Bag,
Suva,
Fiji,
Telephone: +679 337 0733
Fax: +679 337 0021

SPC Pohnpei Regional Office
PO Box Q,
Kolonias, Pohnpei, 96941 FM,
Federated States of Micronesia
Telephone: +691 3207 523
Fax: +691 3202 725

SPC Solomon Islands
Country Office
PO Box 1468
Honiara, Solomon Islands
Telephone: + 677 25543 /
+677 25574
Fax: +677 25547

Email: spc@spc.int
Website: www.spc.int